https://doi.org/10.5194/egusphere-2025-615
Preprint. Discussion started: 28 March 2025

Investigating firn structure and density in the accumulation area of Aletsch Glacier using Ground Penetrating Radar

Akash M Patil[1,2], Christoph Mayer[2], Thorsten Seehaus[1], and Alexander R. Groos[1]

[1]Institute of Geography, Friedrich-Alexander-Universität Erlangen-Nürnberg, 91508 Erlangen, Germany
[2] Bavarian Academy of Sciences and Humanities, Geodesy and Glaciology, Alfons-Goppel Str. 11, D-80539 Munich, Germany

Correspondence: Akash M Patil (akash.patil@badw.de / akash.patil@fau.de)

Abstract. The role of firn structure and density in geodetic glacier mass balance estimation has been constrained, with studies in alpine conditions primarily relying on models. Our research focuses on understanding firn structures and firn density-depth profiles in the Aletsch Glacier's accumulation area using field methods, Ground-Penetrating Radar (GPR) as a geophysical tool, glaciological methods, and firn compaction models. We aim to characterize the firn structure and determine the spatial firn density-depth profiles by estimating electromagnetic wave velocities. Identifying reflection hyperbolae via semblance analysis from common midpoint (CMP) data sets are used for this purpose. Three density-depth profiles, up to 35 m depth, were obtained at various locations within the accumulation area. The Ligtenberg (LIG) and Kuipers Munnekee (KM) firn compaction models were selected from the community firn models (CFM) to evaluate how well the model results matched the observations. These models were adjusted to fit the estimated 1-D firn density profiles from CMP gathered by optimising model coefficients based on regional climatic conditions.

We developed a method to estimate accumulation history by chronologically identifying GPR-derived internal reflection horizons (IRHs) as annual firn layers, validated against estimated snow water equivalent (SWE) from long-term stake measurements. Our findings emphasize the importance of direct measurements, such as snow cores, firn cores, and isotope samples, in identifying the previous summer horizon. We investigated the spatial firn density distribution and the glacier's accumulation history over the past 12 years using a 1.8 km GPR transect, supported by CMP-derived density-depth profiles. Our study underscores the potential of integrating GPR, direct measurements, and firn compaction models in monitoring firn structures and density, ultimately enhancing glacier mass balance estimation in future research.

1 Introduction

Mountain glaciers connote the effect of climate change along with their local hydrology and ecological significance (Haeberli, 1998; Kaser et al., 2006; Stocker et al., 2013). Glaciers across the globe are monitored by studying their mass balance to comprehend the response and adjustment to climate change and provide information on the water sources (Barry, 2006; Kaser et al., 2006; Ohmura et al., 2007; Zemp et al., 2009). It is well known that the glacier mass balance can be estimated accurately in the ablation area whereas, the inadequacy of accumulation measurements leads to the under-representation of spatial glacier mass changes (Østrem and Brugman, 1991). Geodetic approaches are an important and efficient way to estimate the glacier

https://doi.org/10.5194/egusphere-2025-615
Preprint. Discussion started: 28 March 2025

volume change mainly of alpine glaciers and glacierized mountain regions (Sapiano et al., 1998; Cuffey and Paterson, 2010; Huss et al., 2014). Satellite and airborne surface elevation change data estimate the glacier and ice sheet volume changes up to centimetre-scale resolution (Wingham et al., 1998; Zwally et al., 2005; Helm et al., 2014). However, there is a need to convert this volume change to mass change. One approach involves assuming a constant conversion factor of 850±60 kg m^{-3} (Huss, 2013) while taking into account the varying amounts of snow and firn relative to the glacier size. Most studies consider constant densities each for the glacier's accumulation and ablation area (600 kg m^{-3} in the firn zone and 900 kg m^{-3} the ablation zone) to derive mass balance from zonal surface elevation changes (e.g. Schiefer et al., 2007; Moholdt et al., 2010; Kääb et al., 2012; Bolch et al., 2013).

As exemplified in many geodetic studies, uncertainties in converting the glacier volume to mass change by assuming a constant density value are susceptible to inaccuracy in the accumulation area where the firn densification processes are poorly constrained (e.g. Gardelle et al., 2012; Kronenberg et al., 2016). Even with density assumptions, uncertainties in the mean glacier mass balance can arise from long-term firn compaction. Thus, understanding the processes influencing the firn stratigraphy in the accumulation area is highly important. The processes such as overburden pressure from accumulated fresh snow and the formation of ice lenses due to melting and refreezing within the firn body alter the firn stratigraphy, reflecting changes in climatic conditions (Benson, 1996). In addition, studies like Jordan et al., 2008 show that the percolation and refreezing of meltwater results in spatial alteration of snow and firn structures.

Comprehension of the firn density structure has many glaciological applications such as estimating glacier mass changes (Shepherd et al., 2012), firn core studies to determine its age (Bender et al., 1997; Blunier and Schwander, 2000) and the surface meltwater hydrology in the case of mountain glaciers (Stevens et al., 2024). Radar-based subsurface mapping (Waddington et al., 2007; Eisen et al., 2008) can reveal the spatial variability of accumulation rates. Interpretation of the seasonal surface elevation change (Zwally et al., 2002; Ligtenberg et al., 2014) is associated with firn compaction, dynamic thinning and surface mass balance (e.g., Wouters et al., 2015). Earlier research provided the fundamental understanding of the firn densification processes in sub-zero climatic conditions (e.g. Herron and Langway, 1980; Arthern and Wingham, 1998; Li and Zwally, 2004; Reeh, 2008; Ligtenberg et al., 2011), but not many studies have looked at the firn densification in temperate glaciers where the rate of firn densification is significantly higher than in cold firn (Kawashima and Yamada, 1997; Cuffey and Paterson, 2010)). Firn densification on mountain glaciers can be influenced by the presence of refrozen meltwater within the pore spaces (Schneider and Jansson, 2004) and the cooling of the uppermost firn layers during the winter season (Hooke et al., 1983).

Previous studies have shown that glaciological methods like snow pits represent pragmatic and complete annual accumulation conditions (Mayer et al., 2014), firn cores provide information such as ice layer patterns due to accumulation and surface melt (Machguth et al., 2016; Rennermalm et al., 2022). Findings of various studies (e.g., Parry et al., 2007; Dunse et al., 2008; Brown et al., 2011; Marchenko et al., 2017; Heilig et al., 2020) have revealed the local variability of snow depths, firn densification rates and long term accumulation rates. However, each method has pros and cons concerning the effort and vertical resolution required to analyse the stratigraphy. Methods like isotope sample analysis better allow the identification of the annual layers (Aizen et al., 2005) within the firn body. Still, they are constrained to the colder climate owing to the effect of melting processes in temperate conditions resulting in the dispersion of isotope samples (Hou and Qin, 2002). The main drawback of

https://doi.org/10.5194/egusphere-2025-615
Preprint. Discussion started: 28 March 2025

these conventional glaciological studies is the time required for excavating the snowpit or firncore samples which non-invasive geophysical methods can compensate.

Ground-penetrating radar (GPR) has been effectively used in various glaciological applications, such as snow-accumulation studies in Antarctica (Sinisalo et al., 2003), firn and ice transition in a polythermal glacier in Svalbard (Pälli et al., 2003), and estimation of firn density in the percolation zone of the western Greenland ice sheet (Brown et al., 2012). Additionally, it has been utilized to study firn stratigraphy in Svalbard (Marchenko et al., 2017) and for accumulation and thickness measurements of Alpine and high-altitude glaciers (e.g., Machguth et al., 2006; Bauder et al., 2018; Lambrecht et al., 2020). The GPR's ability to detect the change in dielectric permittivity and electric conductivity between two mediums, the ease with which it can be used and the possibility of having repeat measurements due to its non-invasive behaviour (Davis and Annan, 1989; Fisher et al., 1992; Arcone and Kreutz, 2009) make it the preferred technique over other geophysical methods. According to Vaughan et al., 1999 and Helm et al., 2007, the visualised internal reflection horizons (IRHs) within the firn body from the GPR are perceived to be isochrones. Common midpoint (CMP) GPR measurements are usually used to obtain the radar propagation velocity as a function of depth which provides a better estimation of IRHs depths seen on radargrams (e.g., Hempel et al., 2000; Brown et al., 2011). Several studies have demonstrated the ability to determine the water equivalent (w.e.) between the IRHs using radar data in cold conditions (e.g. Kohler et al., 1997; Kruetzmann et al., 2011; van Pelt et al., 2014). Sold et al. (2015) studied helicopter-based GPR measurements to unlock the firn annual water equivalent in temperate conditions. However, the study does not consider the importance of radar velocity to get the IRHs depths.

Huss (2013) emphasizes the importance of spatial firn volume and density distribution in estimating mountain glacier mass balance from the volume measured using geodetic methods. Therefore, in this study, we explore the firn structure and firn density distribution using the GPR-based CMP method, alongside established glaciological methods, in the accumulation area of the Aletsch glacier in the Swiss Alps. We identified IRHs on radargrams as annual firn layers by comparing them with yearly stake-estimated snow water equivalent (SWE), aiding in tracking the accumulation history. We also obtained a long GPR transect to monitor the spatial distribution of the firn layering. We tracked the depth to the first summer horizon using glaciological measurements, which is crucial to validate the GPR-derived results. The geophysical results lay the foundation for testing and calibrating firn compaction models selected from the community firn model (CFM, Stevens et al., 2020). By doing so, we aim to evaluate their accuracy under specific climatic conditions and their usefulness for future research. Consequently, we illustrate the application of GPR and highlight the significance of the CMP method in investigating the spatial variation in firn stratigraphy and density structure, as well as in retrieving the accumulation history of the firn area, exemplified at the Aletsch glacier.

2 Study area and Data acquisition

2.1 Study area

In search of an alpine glacier with a thick and extensive firn body, we selected the Aletsch glacier in the Swiss Alps as a study area for this research, which has good accessibility from the High Altitude Research Station Jungfraujoch. With an area of

https://doi.org/10.5194/egusphere-2025-615
Preprint. Discussion started: 28 March 2025

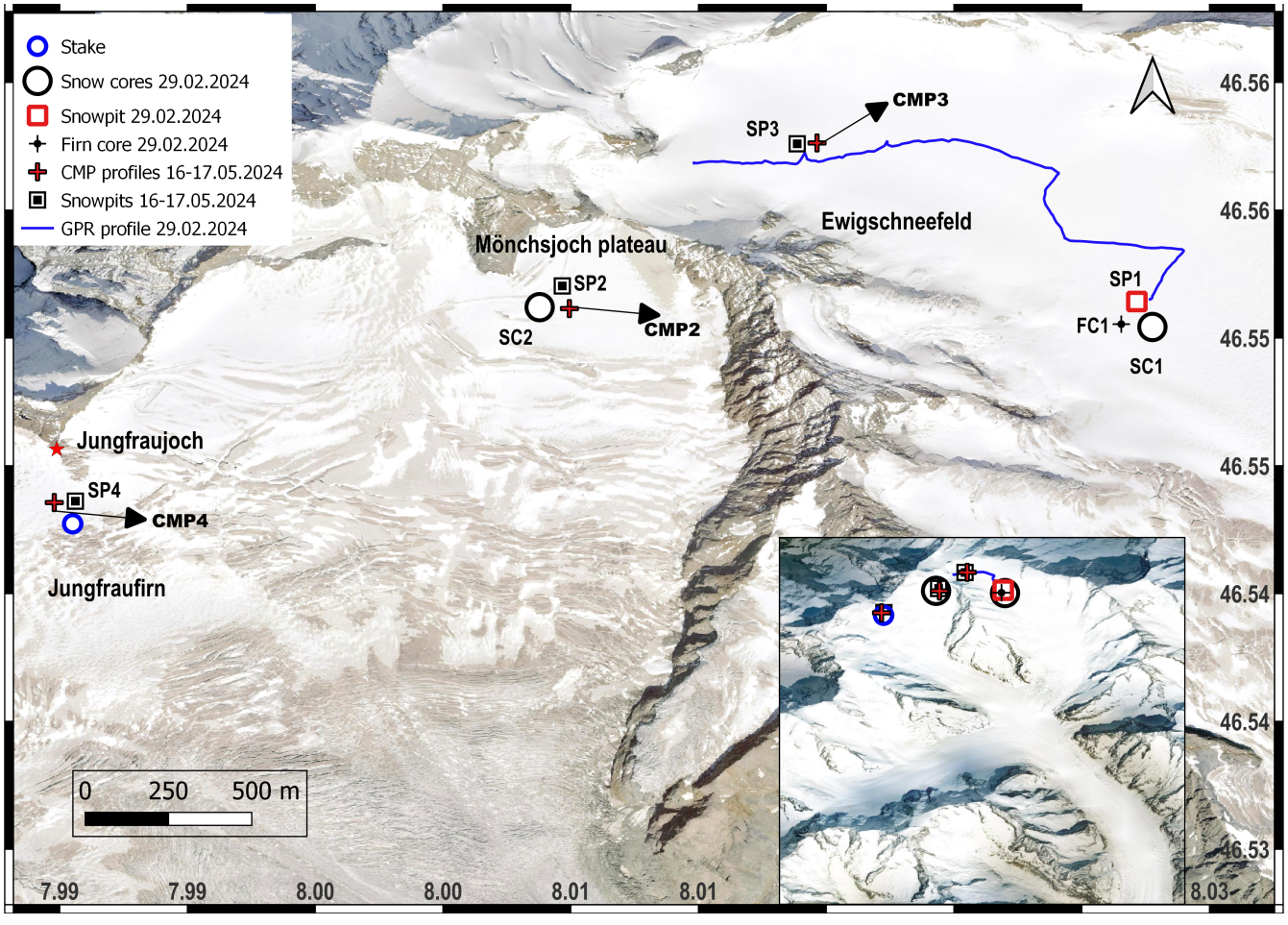

Figure 1. The study area with the geophysical and glaciological measurements on two of the accumulation basins of the Aletsch glacier. Snow pits (SP1), a firn core (FC1), and snow cores (SC1 and SC2) were obtained from the Ewigschneefeld and Mönchsjoch along with the GPR profile during the February-March 2024 measurements. The three Common Mid Point measurements (CMP2, CMP3 and CMP4) and shallow snow pits (SP2, SP3 and SP4) were gathered during 16-17 of May 2024 at Mönchsjoch, Ewigschneefeld and Jungfraufirn (near the Stake) respectively. The inset map illustrates an oblique satellite view of the Aletsch glacier during the winter of 2024 (© Google satellite map). The background map is a cloud-optimised GeoTIFF of 2 m resolution provided by the Swiss Federal Office of Topology, © swisstopo 2024.

https://doi.org/10.5194/egusphere-2025-615
Preprint. Discussion started: 28 March 2025

Table 1. The GPR antenna settings used for the GPR profile and CMP measurements during the winter campaign 2024.

Acquisition date	29 February 2024	16-17 May 2024
Type of acquisition	GPR profile	CMP gather
Antenna frequency (MHz)	200 and 600	500
Number of samples	2048	500
Time window (ns)	400	400
Trace increment (m)	0.0176	0.2
Time increment (s)	0.195	0.2

about 80 km^2, a length of about 20 km and a maximum thickness of around 800 m, Aletsch glacier is the biggest glacier in the European Alps (Farinotti et al., 2009; GLAMOS, 2018). Aletsch glacier ranges from 1700 to 4200 m a.s.l. and comprises about 20% of the total glacier volume in the Swiss Alps (Bauder et al., 2007). Accumulation areas of the glacier consist of Grosser Aletschfirn in the west, Jungfraufirn in the north, and Ewigschneefeld in the northeast (Fig. 1). According to meteorological data recorded at Jungfraujoch research station at an elevation of 3580 m a.s.l, the mean annual temperature of the last three decades (1991-2020) was -6.7 °C and the mean daily temperature from the September-June period was well below 0 °C (MeteoSchweiz, 2024). An accumulation stake is located on the glacier at an elevation of 3390 m a.s.l., near the Jungfraujoch. It was installed in 1918 and has presented continuous annual glaciological measurements records since then (GLAMOS, 2018). The glacier has been extensively studied since the 1940s (e.g. Seligman, 1941) and it provides an archived glaciological and other in situ data set to validate our current measurements as in the World Glacier Monitoring Service (WGMS).

2.2 Data acquisition

2.2.1 GPR data

On 29 February 2024, a 1.8 km long GPR transect was measured on the Ewigschneefeld (Fig. 1) using the IDS monostatic 200 and 600 MHz dual-frequency, shielded GPR system. The choice for the location of the GPR profile was to repeat the measurements done by Bannwart et al. (2024) for future studies. Three sets of crossed CMP profiles at a right angle were gathered at three different locations of the upper Aletsch glacier, i.e. at the Jungfraufirn (near the Stake in Fig.1), the Mönchsjoch plateau and the Ewigschneefeld on 16-17 May 2024. The measurements were carried out using the PulseEkko mono-static 500MHz GPR system consisting of a separate shielded transmitter and receive antenna. At each spacing of the GPR antennas, radar pulses were triggered manually twice with 128 stacks per trace. The initial distance between the two antennas was 20 cm. The transmitter and receiver were moved along a straight line, maintaining a constant offset of 20 cm over a length of 20 m, with a step size of 10 cm on either side of a common midpoint. However, this study includes only an analysis of parallel CMP profiles from each location. Table 1 shows the general GPR settings used.

https://doi.org/10.5194/egusphere-2025-615
Preprint. Discussion started: 28 March 2025

2.2.2 Glaciological investigations

A 4 m deep snow pit was dug at the Ewigschneefeld on 29 February 2024. The snow density was measured using a 17 cm long metallic cylinder of approximately 4 cm in diameter, which resulted in a vertical resolution of 17 cm. A shallow firn core of 3.8 m deep from the bottom of the snow pit was drilled to a total depth of 7.8 m using a "Mark II Ice Coring System" from Kovacs Ice Drilling Equipment with a diameter of 9 cm. The density was measured at a 20 cm depth interval on the core. Another shallow snow core of 5.8 m was obtained a few meters away from the snow pit, to allow a direct comparison between the snow/firn core and snowpit measurements (Fig. 1). Another snow core of 5.4 m long was recovered from the Mönchsjoch plateau on 2 March 2024, applying the same vertical resolution for the density measurements. In addition, isotope samples were collected every 20 cm from the snow cores and snow pit at both locations to identify the depth of the last summer horizon. Similarly, snow pits were dug at the Mönchsjoch plateau (1.3 m deep), Ewigschneefeld (1.9 m deep), and Jungfraufirn (1.9 m deep) on 16 and 17 May 2024 (Fig. 1).

3 Methods

3.1 GPR data processing

The GPR data acquired during the field campaign were processed using the ReflexW software (Sandmeier Scientific Software), following a traditional processing sequence (Ulriksen, 1982; Annan, 1993; Fisher et al., 1996). We applied a sequence of filters and gains to remove apparent noise and improve the visibility of the IRHs on the radargrams, such as moving the start time to get the first arrival at the surface, applying a de-wow filter, stacking, and using a bandpass Butterworth filter to increase the signal-to-noise ratio, as well as background removal and static corrections to reduce system-induced irregularities (Fig. 2). The IRHs seen on radargrams were picked using the built-in, semi-automatic phase follower tool. The radar propagation velocity was assumed to be constant at 0.21 m ns^{-1} (Looyenga, 1965) to visualize the radar penetration depth within the firn body (Fig. 2, right axis).

3.2 GPR CMP semblance analysis

The physical properties of the subsurface are derived from the radar wave propagation velocity, facilitating the estimation of reflector depth by converting the travel time to depth in the radargram through the dielectric mixing model (Looyenga, 1965; Topp et al., 1980; Endres et al., 2009). The common-midpoint (CMP) method is an acquisition approach keeping an identical distance between the transmitter (Tx) and the profile centre, as well as the receiver (Rx) and the profile centre at all positions along the acquisition. Velocities are estimated by matching the curvature of diffraction reflections from the subsurface targets assuming horizontal homogeneous layers (Yilmaz, 2001; Annan, 2005; Porsani and Sauck, 2007; Schmelzbach et al., 2012). The CMP data were analysed using the semblance analysis which measures the coherence of energy between waveforms within the analysis windows centred on hyperbolic trajectories (Sheriff and Geldart, 1999).

https://doi.org/10.5194/egusphere-2025-615
Preprint. Discussion started: 28 March 2025

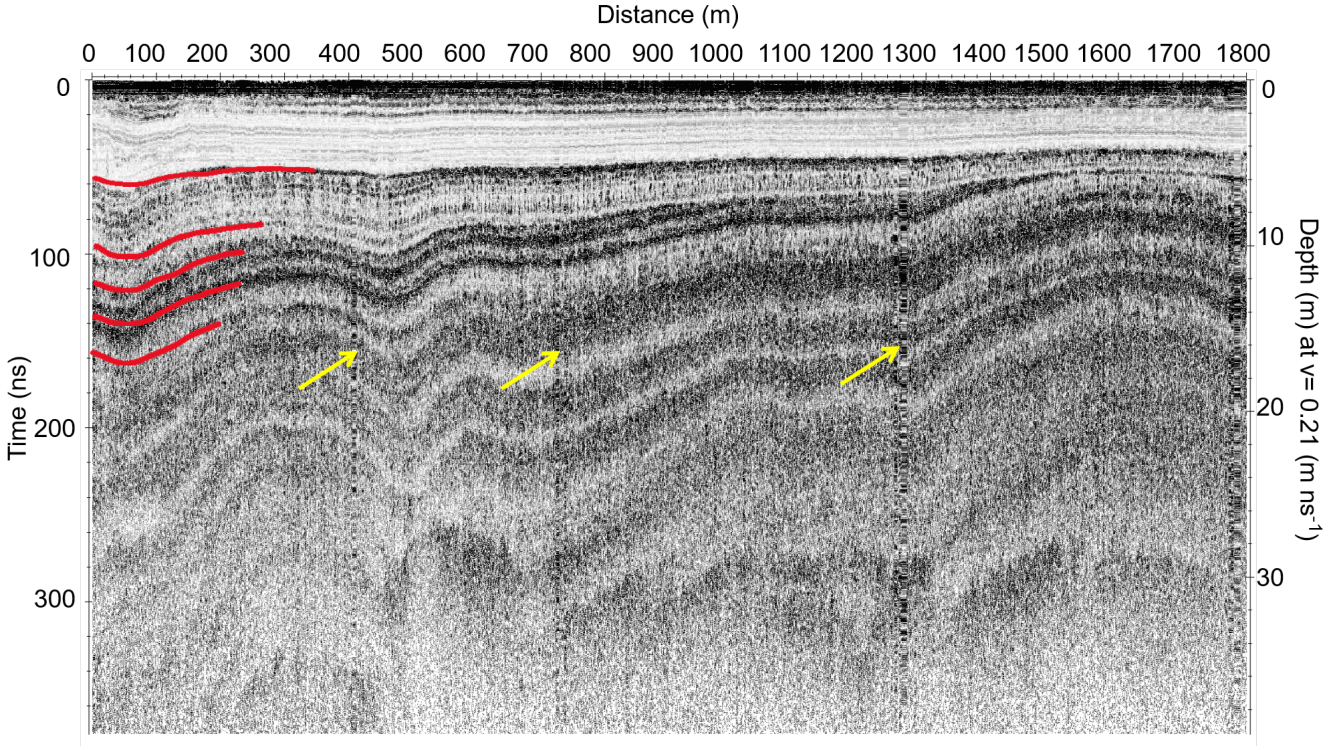

Figure 2. Radargram at Ewigschneefeld from 29 February 2024. The GPR profile runs from higher (left) to lower elevation (right). Yellow arrows indicate the artefacts from stops during the measurements. The red lines indicate prominent IRHs and potential annual layers at different depths.

To estimate the depth of IRHs, the GPR CMP profiles were analysed using the CMP (1D) analysis module within ReflexW software. The initial processing of gathered CMP data was done according to the processing of the GPR profile (sect 3.1). The linear approximation of the direct wave with an assumed wave velocity of 0.3 m ns^{-1} is shifted to zero offsets at its starting point for the static time correction. The semblance analysis was run after setting up the input parameters within the interactive adaptation module and the un-normalized correlation section. The correlation histogram can be seen on the right side of Fig 4. The best fitting velocity can be chosen on the correlation histogram, by comparing the calculated hyperbolas with the measured hyperbolic reflections. This process continues for all identified layers (red lines in Fig. 4). Sandmeier's geophysical research - ReflexW user guide (Sandmeier version 5.0) provides a detailed comprehension of the semblance analysis. The velocity-depth profile estimated from CMP data was used to derive the corresponding density-depth profile by adapting the complex refractivity index method CRIM (Wharton et al., 1980; Knight et al., 2004) as

$$\rho = \frac{\left(\frac{V_{\text{air}}}{V_{\text{firn}}} - 1\right)}{\left(\frac{V_{\text{air}}}{V_{\text{ice}}} - 1\right)} \rho_{\text{ice}} \tag{1}$$

https://doi.org/10.5194/egusphere-2025-615
Preprint. Discussion started: 28 March 2025

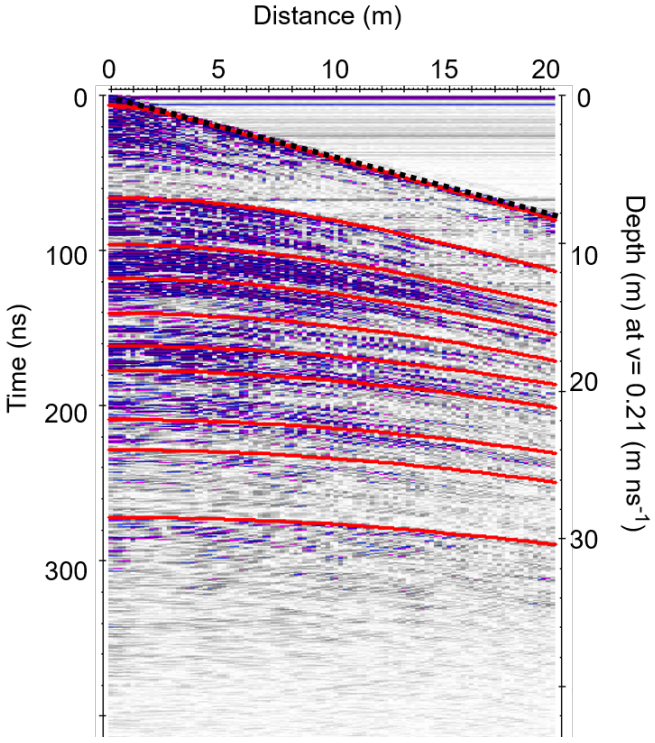

Figure 3. The processed GPR CMP data gathered at Ewigschneefeld on 17 May 2024. The 20 m long CMP profile depicts various hyperbolic reflections, visible down to a depth of 30-32 m. The left y-axis shows the two-way travel time (twt) in ns, while the right y-axis indicates an approximate depth, assuming a constant radar velocity in firn of 0.21 m ns^{-1}. The direct wave (black dotted line) and identified hyperbolic reflectors (solid red lines) are indicated at different depths.

Equation 1 illustrates the dependency of the radar-wave velocity on the density. Here, V_{air}, V_{ice} are radar wave propagation velocities in air and ice (0.3 and 0.17 m s^{-1} respectively), whereas the velocity of the radar wave within the firn layer (V_{firn}) was estimated from the CMP semblance analysis.

3.3 Firn densification modelling

Firn densification models help convert measured glacier volume change to mass change and understand the rheological properties and firn density-depth profiles within mountain glaciers and ice sheets consisting of a thicker firn body (Gagliardini and Meyssonnier, 1997; Lüthi and Funk, 2000). This study primarily examines observation-derived results to investigate firn structure and densification in temperate alpine conditions. By testing and calibrating firn densification models, we aim to evaluate their accuracy under specific climatic conditions and their usefulness for future research.

https://doi.org/10.5194/egusphere-2025-615
Preprint. Discussion started: 28 March 2025

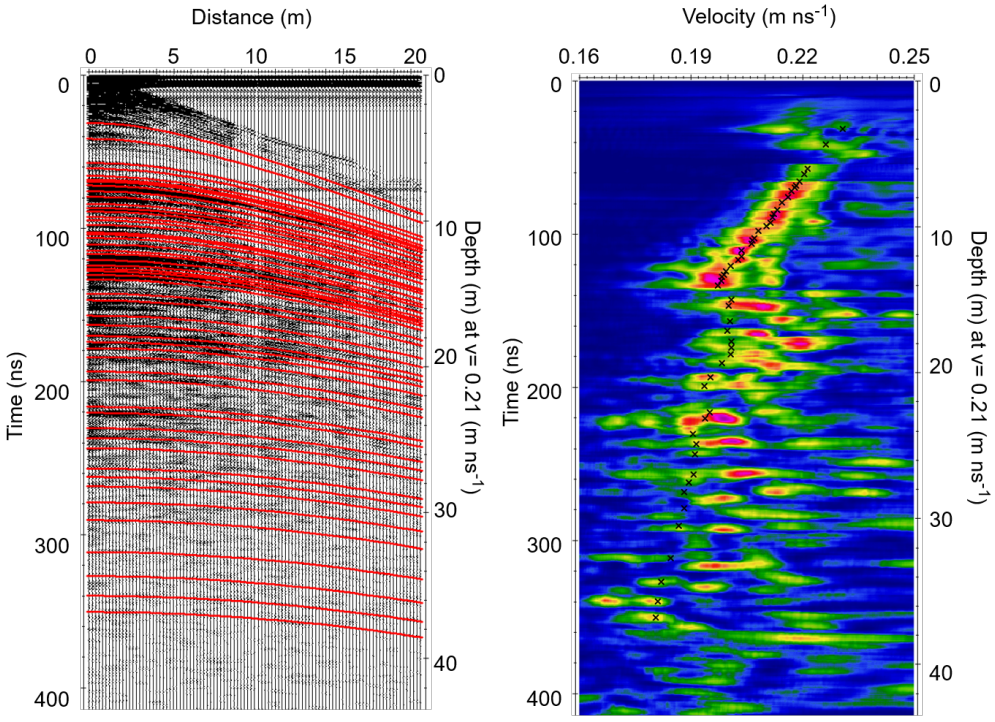

Figure 4. The Semblance analysis using ReflexW software presents the picked energy coherence (right) matching the hyperbolic pattern or IRHs (left) obtained from the CMP gathered at Ewigschneefeld (Fig 1). Even though the energy coherence is high, the hyperbolic reflections are unnoticeable at deeper depths (> 30 m).

3.3.1 Community Firn Model for Firn Densification

The Community Firn Model (CFM), developed by Stevens et al. (2020), is used in this study to model firn densification using regional climate data. CFM is an open-source firn model framework that can run 13 previously published models. It allows users to choose the simulation modular run for particular physical processes to obtain results for the selected module. More details about the CFM workflow can be found in Stevens et al. (2020). We used the Ligtenberg (LIG) and Kuiper Munneke (KM) models, developed to simulate one-dimensional firn densification, considering meltwater percolation and refreezing processes, mainly in Antarctica and Greenland, respectively (Stevens et al., 2020). Generally, both models require accumulation rate and air temperature as input parameters and consider potential melting and refreezing processes in the simulations. LIG is an empirical approach based on observations from ice cores, providing the general firn densification trend (Ligtenberg et al., 2011). The LIG and KM models are based on Arthern et al. (2010) and differ only in their coefficients, representing different sensitivities of densification processes, as shown in Equation 2 and 3.

We adopted the same parameters for tuning (Table 2), to fit the observed density-depth profile from glaciological and geophysical methods. The models were run for two elevations, 3600 and 3400 m a.s.l., representing the approximate elevations of

https://doi.org/10.5194/egusphere-2025-615
Preprint. Discussion started: 28 March 2025

Table 2. The LIG and KM model parameter coefficients (Eq 2 and 3) and the tuned values to fit the observational results

Coefficients	LIG	KM	Our values
α_1	1.435	1.042	1.5
α_2	2.366	1.734	2.4
β_1	0.151	0.0916	0.09
β_2	0.293	0.2039	0.35

Mönchsjoch and Ewigschneefeld, to consider air temperature differences between both locations while keeping the precipitation rate constant. The model spin-up period was set for 100 years, during which the models ran over 10 years (2005-2015) forcing data repeatedly to reach a steady state. After this period, the models used daily input data for simulating the firn density evolution under an assumed constant surface snow density of 300 kg m^{-3}.

The general formulation of firn densification in the chosen models assumes a logarithmic relationship with respect to the accumulation rate and an exponential relationship concerning the inverse temperature. The coefficients differ for snow densification (density < 550 kg m^{-3}) and firn densification (density > 550 kg m^{-3}). The general form of this relationship is

$$C_0 = \Big(\alpha_1 - \beta_1 \ln(\dot{b})\Big)\left(0.07\dot{b}g\exp\left(-\frac{E_c}{RT}+\frac{E_g}{RT_m}\right)\right) \quad \text{for } \rho \leq 550 \text{ kg m}^{-3} \tag{2}$$

$$C_1 = \Big(\alpha_2 - \beta_2 \ln(\dot{b})\Big)\left(0.03\dot{b}g\exp\left(-\frac{E_c}{RT}+\frac{E_g}{RT_m}\right)\right) \quad \text{for } \rho \leq 550 \text{ kg m}^{-3} \tag{3}$$

where, $(\dot{b})$ is the accumulation rate in kg m^{-2} a^{-1}, g is the acceleration due to gravity (9.80 m s^{-2}), while E_c and E_g represent the activation energy for diffusion and grain growth respectively (60 and 42.4 kJ mol^{-1}). T_m represents the mean surface temperature in Kelvin as described in Ligtenberg et al. (2011) and Simonsen et al. (2013). The coefficients $\alpha_{1,2}$, $\beta_{1,2}$, and $\gamma_{1,2}$ are as in the Table 2 for the two models and our optimization:

3.4 Input parameters for firn densification model

3.4.1 Climate forcings data

The necessary climate forcings for the CFM runs, such as the daily mean temperature, were obtained from the Jungfraujoch weather station at 3580 m a.s.l. (MeteoSchweiz, 2024). Due to high winds and snow drift, precipitation data is not available from the Jungfraujoch research station. Therefore, daily mean precipitation data was used from observations at the Grimsel research station, situated at 1952 m a.s.l., approximately 25 km northeast of our investigation site at Aletsch glacier. The precipitation data were scaled to the Jungfraujoch elevation using a simple statistical approach (section 3.4.2). Air temperature data were adjusted to the respective elevation using a constant lapse rate of 6.5 °C km^{-1}.

We estimated the seasonal melt factor by dividing the sum of SWE during the melting period (1 May to 31 August) each year by the sum of positive daily mean temperatures during the same period. Figure 7 shows the estimated melt factors over the last

https://doi.org/10.5194/egusphere-2025-615
Preprint. Discussion started: 28 March 2025

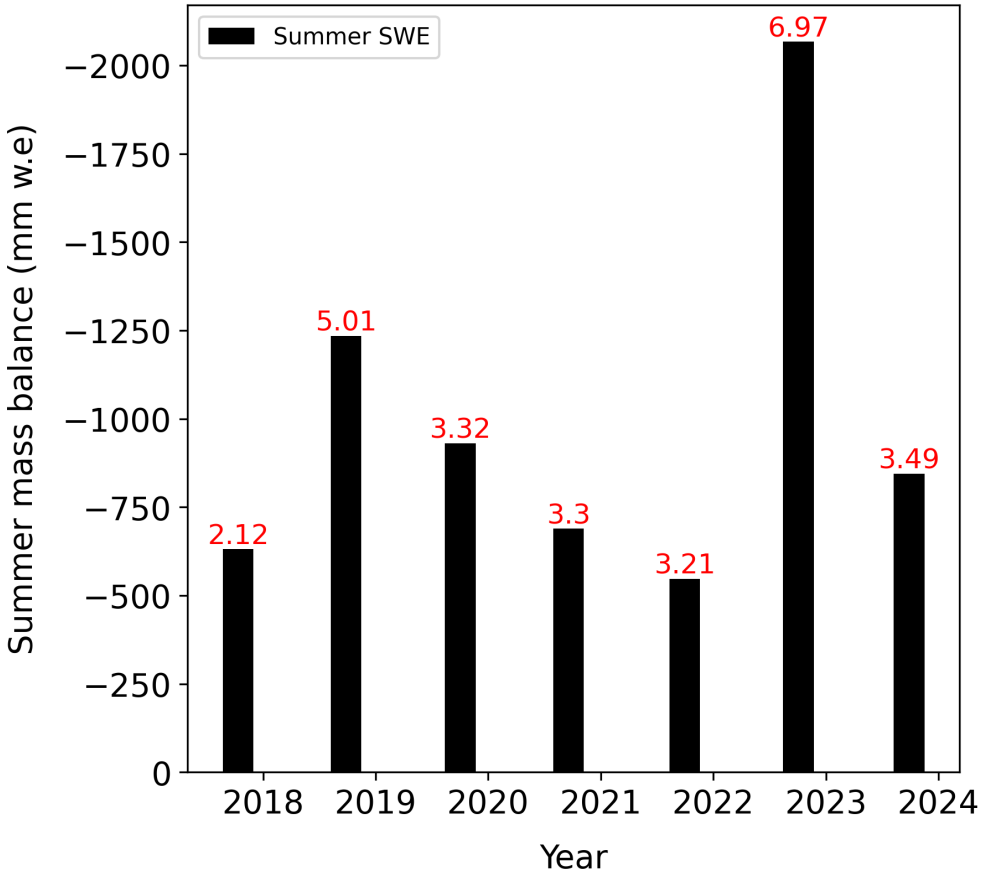

Figure 5. Ablation measured at the stake on Jungfraufirn (Fig. 1) during the melting period (black bars) and estimated corresponding degree day factor or melt factor in mm $^{\circ}C^{-1}$ day^{-1} (red numbers) shown here are considered to determine a daily melt rate for the CFM input force.

seven years, resulting in a mean melt factor of approximately 3.9 mm $^{\circ}C^{-1}$ day^{-1} and a maximum of 6.9 mm $^{\circ}C^{-1}$ day^{-1} during the peak melting period of 2022. This snowmelt rate value falls within the general assumption of 2.7-11.6 mm $^{\circ}C^{-1}$ day^{-1} according to Hock (2003). As most ice sheet modelling studies use a melt factor of 3 mm $^{\circ}C^{-1}$ day^{-1} (e.g., Wake and Marshall, 2015), we tested the model's behaviour for a melt factor of 3.5 mm $^{\circ}C^{-1}$ day^{-1}. Furthermore, sensitivity tests were also performed for two melt factor of 5.5, and 8.5 mm $^{\circ}C^{-1}$ day^{-1}.

3.4.2 Scaling precipitation data

The precipitation data from the Grimsel meteorological station at an elevation of 1952 m a.s.l was scaled to an elevation of our study area of 3600 m a.s.l. The following method of Cullen and Conway (2015) was used to get the daily mean precipitation data at Aletsch Glacier from Grimsel weather station. No precipitation data was recorded from Grimsel weather station from 31 December 2011 till 30 November 2012. This data gap was filled by the mean winter daily precipitation data from 2004 to

https://doi.org/10.5194/egusphere-2025-615
Preprint. Discussion started: 28 March 2025

2024. The daily rainfall data available at Grimsel can be linearly translated into daily SWE using the UBC Watershed Model that employs the gentle variation in the rain and snow proportion as given in Eq. 4 (Pipes and Quick, 1977).

$$\begin{aligned} &\text{for } T \leq 0.6°\text{C} && : \text{all precipitation is considered as snow} \\ &\text{for } 0.6°\text{C} < T < 3.6°\text{C} && : \text{rain proportion} = \tfrac{T}{3} - 0.2 \\ &\text{for } T \geq 3.6°\text{C} && : \text{all precipitation is considered as rain} \end{aligned} \tag{4}$$

Here, T is the mean daily air temperature. The snowfall at Grimsel is available as cumulative daily snow height (HS in cm), which was converted to SWE (in mm) using the Delta Snow Model, as demonstrated in a recent study by Winkler et al. (2021). Thus, the obtained daily SWE represents the daily snowfall. The attained snowfall at Grimsel is summed up over the accumulation period (1 September to 31 May) each year to obtain a seasonal SWE. From the measured cumulative SWE data during the accumulation period at Jungfraufirn (Sect. 2.1), we derived the scaling factor of SWE for each year, as shown in Equation 5. The daily mean snowfall at the Grimsel research station was multiplied by the estimated scaling factor to obtain the daily mean precipitation at the Aletsch glacier. Furthermore, the rain precipitation at Grimsel was added to the snowfall to determine the daily mean precipitation at the Aletsch glacier, considering the rain at Grimsel as snow in the accumulation basins of the Aletsch glacier. The analysis of the SWE estimation at the Grimsel automatic weather station (AWS) yields a trend similar to that of the stake-derived SWE at the Aletsch glacier. Figure 6 provides the validation of the method to scale the daily precipitation from Grimsel to Aletsch glacier.

$$SF = \frac{\text{SWE}_{\text{stake\_winter}}}{\text{SWE}_{\text{Grimsel\_winter}}} \tag{5}$$

3.5 IRHs as firn layers

To identify IRHs as annual firn layers, there must be more than one IRH on the radargram, and the distinguishable IRHs between the uppermost and lowermost IRH are also important. Within all three CMP data sets, we identified more than 25 IRHs (e.g., Fig. 4) in each data set. An iterative method was introduced to identify the picked IRHs as annual firn layers by estimating the SWE between the selected IRHs. This method uses the relationship of SWE with radar wave two-way travel time (TWT), mean layer velocity from CMP semblance analysis, and density between the IRHs (as in Eq. 6). The velocity-depth and density-depth profiles obtained from the acquired CMP data at three accumulation areas of the glacier were used to estimate the SWE at the respective locations.

The TWT between identified IRHs within the acquired CMP profiles was subtracted and multiplied by the estimated layer velocity and density to obtain the SWE within each IRH. The SWE obtained between consecutive layers was validated chronologically against the stake-estimated SWE available at the Jungfraufirn location (Fig. 1, Sect. 2.1) for the particular year. The SWE of the IRHs that matched the corresponding year's SWE from stake-derived values was considered as firn layer of that year. We believe that multiple reflection horizons may occur within a single firn layer due to a change in permittivity. Therefore, IRHs that did not fit the stake-estimated SWE were neglected as firn layers. This process was continued for all available IRHs

https://doi.org/10.5194/egusphere-2025-615
Preprint. Discussion started: 28 March 2025

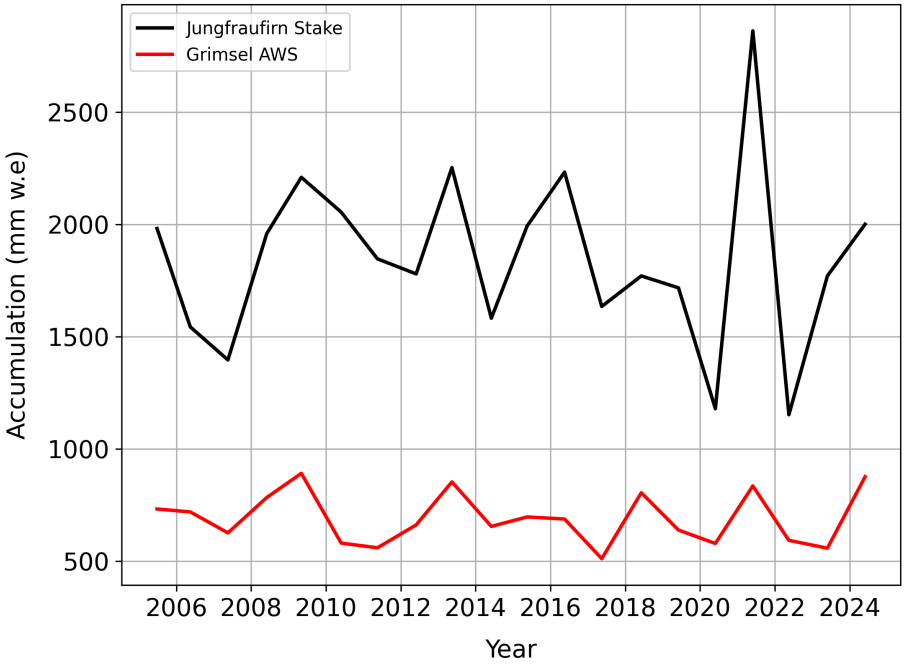

Figure 6. Comparison of the SWE estimation (red) during the accumulation period at the Grimsel Automatic Weather Station (AWS) by translation of the recorded Snow Height (HS) to SWE using the Delta snow model, with the stake measured seasonal SWE at the Aletsch glacier Jungfraufirn (black).

from the CMP radargram. Using this approach, we identified 15 annual firn layers at Ewigschneefeld, 13 at the Mönchsjoch and 8 at Junfraufirn locations (Fig 1).

In the case of the GPR profile gathered at the Ewigschneefeld (Fig. 2), the mean TWT of the IRHs along the profile was considered (Eq. 7, and the difference in TWT of each IRH was used to estimate the SWE of that layer. Here, the layer velocity and density were considered from the CMP gathered at the Ewigschneefeld (CMP3 in Fig. 1).

$$\mathrm{SWE}_{12} = \mathrm{TWT}_{12} \times V_{12} \times \rho_{12} \tag{6}$$

Here, $\mathrm{TWT}_{12} \times V_{12}$ is the thickness of the IRH.

$$\mathrm{TWT}_{12} = \mathrm{mean}(\mathrm{TWT}_{\mathrm{IRH2}}) - \mathrm{mean}(\mathrm{TWT}_{\mathrm{IRH1}}) \tag{7}$$

In the case of IRHs seen on GPR profile radargrams. V_{12} : estimated layer velocity between two IRHs from CMP semblance analysis. and ρ_{12} : estimated density between two IRHs.

https://doi.org/10.5194/egusphere-2025-615
Preprint. Discussion started: 28 March 2025

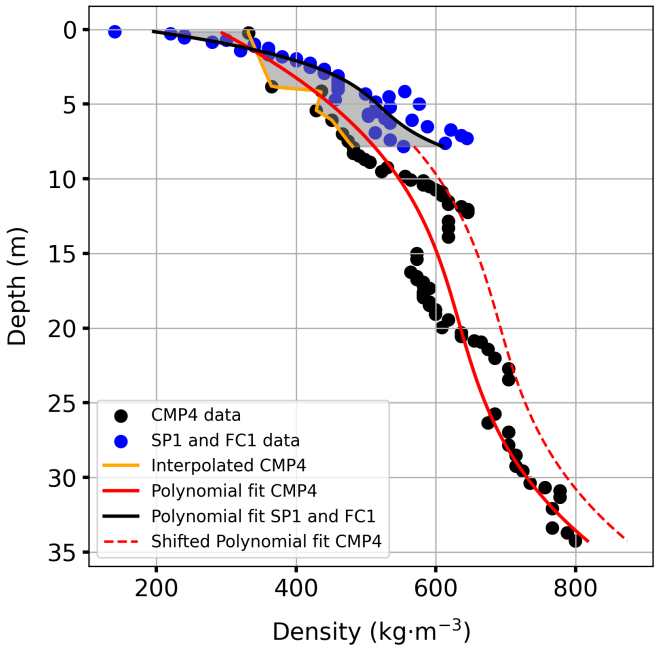

Figure 7. The density-depth trend derived from CMP data (black dots) and snow pit and firn core data (blue dots) at either end of the GPR profile gathered at Ewigschneefeld (Fig. 1) were fitted to the cubic polynomial of degree 3 (solid red line and black line respectively). The density offset between interpolated CMP3 (orange line) and fitted density trends (black line) was estimated (grey fill). The shallow density-depth profile derived from the snow pit and firn core was extended to the deeper depth assuming the cubic polynomial trend (dotted red line) shifted by the estimated average density offset.

3.6 Spatial firn density and accumulation distribution

After identifying the internal reflection horizons (IRHs) as annual firn layers, we used a ground-penetrating radar (GPR) transect at Ewigschneefeld to analyze the spatial variability in firn stratigraphy, density, and accumulation. The GPR profile, approximately 1.8 km long, spans an elevation range from 3550 to 3380 m above sea level. To understand how alpine climatic conditions like precipitation and temperature affect firn densification within this small elevation range, we estimated the spatial distribution of firn density and accumulation. This was done using the CMP-derived density-depth profile at the start of the GPR profile and a shallow density-depth profile (7.8 m) derived from direct measurements at the end of the profile.

The density-depth trend from direct measurements, up to 7.8 m deep (Fig. 8), was fitted with a cubic polynomial (degree 3) to identify the distribution pattern. We then compared this with the CMP-derived density profile up to the same depth to find the density offset (Fig. 7). The average difference between these two profiles was calculated. Furthermore, the CMP-derived density trend was also fitted with a cubic polynomial, showing a good fit with the observations ($R^2 = 0.88$). Due to the lack of density data beyond 7.8 m at the far end of the GPR profile, we assumed that the density trend continues following the cubic polynomial but with the estimated average density offset.

https://doi.org/10.5194/egusphere-2025-615
Preprint. Discussion started: 28 March 2025

The two density trends obtained at either end of the GPR profile were used to track the spatial firn density and accumulation distribution. This was achieved by identifying annual layers and their corresponding depths using the previously described method (Sect. 3.5) and interpolating the density distribution over the 1.8 km transect. The accumulation distribution along the GPR profile was then estimated by multiplying the interpolated density by the thickness of the identified firn layers (Eq. 6).

4 Results

4.1 Glaciological observations

We investigated the origin of the last summer horizon using direct observations from snow pits, snow cores, a firn core, and isotope analysis at two locations of an accumulation area of the Aletsch glacier. Figure 8 shows the density profiles obtained at Mönchsjoch and Ewigschneefeld from the snow pits, snow cores, and a firn core acquired during February-March 2024. The snow cores obtained at these two locations extend to depths of 5.4 and 5.8 m, respectively, illustrating distinct density profiles with a noticeable density offset (nearly 100 kg m^{-3}) in the upper few meters. However, at deeper depths (below 4 m), the density-depth trend is similar at both locations. In Figure 8, kinks can be observed in the density profile at depths of 2 and 3 m (Ewigschneefeld, SC1) and 3.5 m (Mönchsjoch, SC2), attributed to potential melt events due to positive temperatures during early January 2024, late November, and mid-October 2023 (MeteoSchweiz, 2024), respectively.

The data from the 4 m deep snow pit (SP1) next to the snow core (SC1) reveal a linear increase in the density profile without drastic changes (black line, Fig. 8). Further, the 3.8 m firn core (FC1) obtained from the bottom of the snow pit illustrates a similar increasing density trend, with a maximum density of around 640 kg m^{-3} at a depth of 7.3 m. We identified ice lenses within the snow pit (SP1), snow cores (SC1 and SC2), and firn core (FC1) at both locations (Ewigschneefeld and Mönchsjoch), which are more frequent at deeper depths, hinting at the possible effect of seasonal melt and refreezing. Isotope analysis supports the identification of the depth of the last summer horizon. The results in Figure 9 show the fluctuation of the δ^{18}O and δD up to a depth of 5 m, illustrating the temperature variability during precipitation events within the 2023-2024 winter period. Below the 5 m depth, there are no strong variations of isotopic signals, which can be interpreted as the dilution of the isotope signal due to summer melt. We therefore connect this change with the transition to the firn layer of the previous year. With the available results from direct observations and isotope analysis, we assume the last summer horizon at an approximate depth of 4.8-5 m. The snow above the last summer horizon represents the winter precipitation until 29th February 2024 and equals 2000 mm w.e. at Mönchsjoch and 2100 mm w.e. at Ewigschneefeld.

Figure 10 represents the density profiles from the three shallow snow pits dug close to each CMP location to estimate the precipitation rate between 29 February and 17 May 2024. Density profiles obtained from snow pits at Ewigschneefeld (SP3) and Jungfraufirn near the stake (SP4) show similar trends, with densities ranging from 200-460 kg m^{-3} within 2 m of depth. However, due to unfavourable weather on 16 May 2024, only a 1.3 m deep snow pit was dug at Mönchsjoch (SP2), presenting a density range of 240-360 kg m^{-3}. The effect of elevation differences at Mönchsjoch, Ewigschneefeld, and Jungfraufirn is evident from the density profiles, exemplifying the spatial variability in precipitation. It is also observable that ice lenses start at the near-surface level of around 0.25 cm and depth hoar at 0.6-1.5 m, hinting at days with warmer temperatures between

https://doi.org/10.5194/egusphere-2025-615
Preprint. Discussion started: 28 March 2025

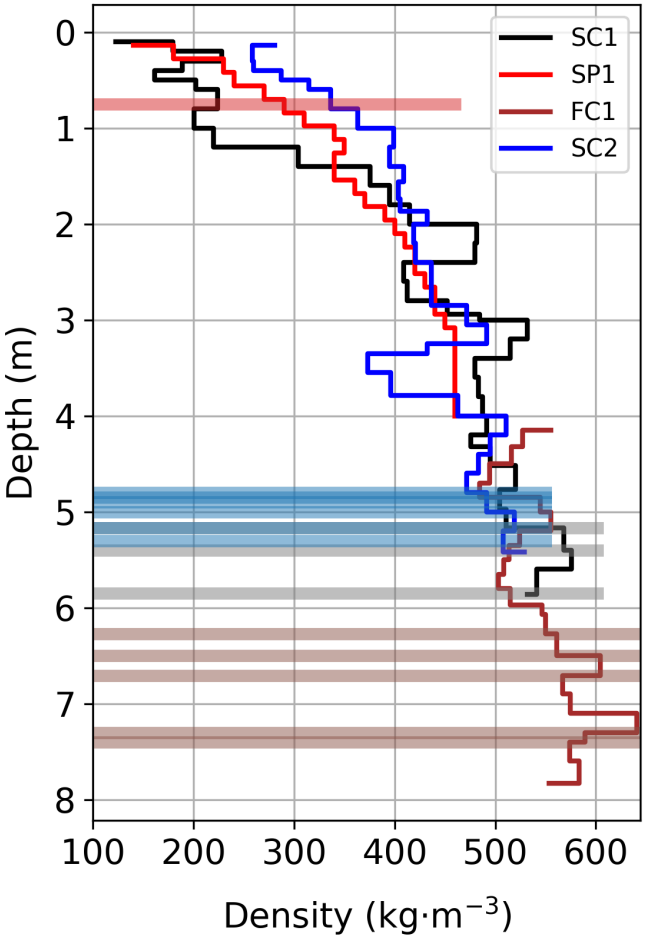

Figure 8. Density-depth profiles obtained from direct measurements using glaciological methods such as snow-pit and firn cores at two locations (sect 2.1). The firn core (FC1) density profile shown by the brown colour was drilled from the bottom of the snowpit (SP1) and depicted as a red line. The black line illustrates the density profile obtained from the snowcore (SC1) drilled a few meters parallel to the snowpit. All these measurements were taken at the Ewigschneefeld (Fig. 1). The blue line is the density profile estimated from the snowcore (SC2) drilled at the Mönchsjoch plateau (Fig. 1). The ice lenses observed at particular depths were denoted in similar coloured horizontal bars. The thickness of observed ice lenses is not to scale.

https://doi.org/10.5194/egusphere-2025-615
Preprint. Discussion started: 28 March 2025

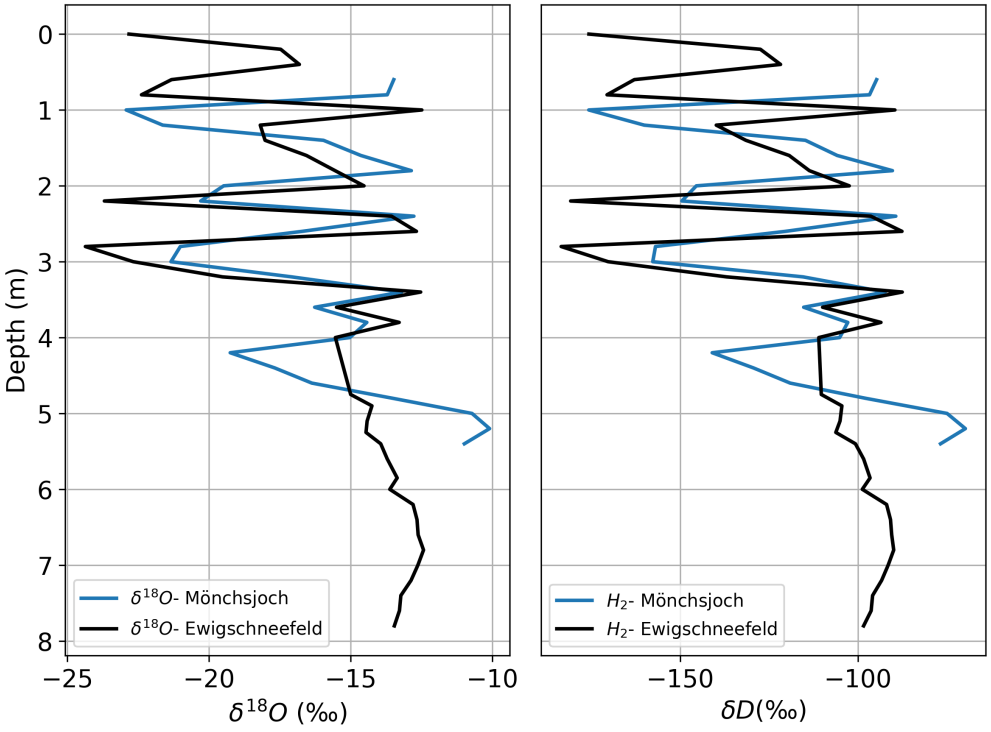

Figure 9. Comparison of δ^{18}O and δD isotope samples gathered from the snow pit (SP1), snow core (SC2), and firn core (FC) at two locations (Ewigschneefeld and Mönchsjoch).

March and May 2024. The snow density does not exceed 360 kg m^{-3} even at 1 m depth near Mönchsjoch (SP2). However, at Ewigschneefeld (SP3) and Jungfraufirn (SP4), snow density reaches 430 kg m^{-3} within 1 m depth, highlighting the spatial change in compaction rate at different locations. Furthermore, the total SWE at SP2, SP3, and SP4 was approximately 420, 740, and 740 mm, respectively.

4.2 GPR-derived firn densification

Figure 11 summarizes velocity-depth and density-depth results from the GPR CMP analysis at three accumulation areas of the Aletsch glacier. Hyperbolic reflections seen on the CMP profiles (e.g., Fig. 3) obtained at three locations (Fig. 1) represent the IRHs within the firn body. The CMP results are used to estimate the 1-D firn density-depth profile (Sect. 3.2). The depth of the deepest discernible reflectors varies between the locations (Fig. 9). Reflection patterns can be seen up to a maximum depth of approximately 35 m at Ewigschneefeld (CMP4), about 32 m at Mönchsjoch (CMP2), and a lower penetration depth of around 22 m at Jungfraufirn near the stake (CMP4). This lower penetration depth can be attributed to the high melt rate at this location compared to the other two CMP locations. Meanwhile, the first pronounced IRH at the three CMP locations was identified at

https://doi.org/10.5194/egusphere-2025-615
Preprint. Discussion started: 28 March 2025

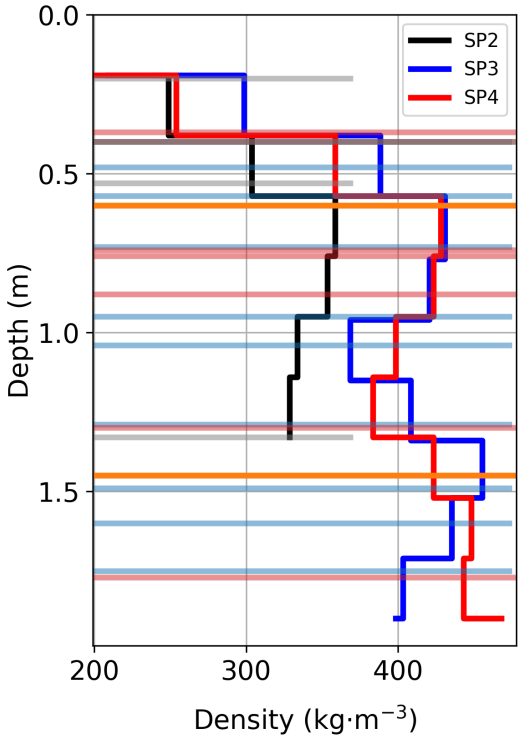

Figure 10. Density-depth profiles obtained from the shallow snow pits dug near each of three GPR CMP profiles (SP2-Mönchsjoch, SP3-Ewigschneefeld and SP4-Jungfraufirn) during the May 2024 measurements. Brown and orange horizontal bars show Sahara dust layers and depth hoar only from the SP3. All ice lenses are shown in light blue colour observed from three snow pits. The thickness of ice lenses, Sahara dust layers and hoar are not to scale.

approximately 3 m depth. The radar wave velocity and firn density fluctuate between 0.23-0.179 m ns^{-1} and 370-800 kg m^{-3} with depth and location, respectively.

The comparison of the results from the three CMP analyses highlights the increased density-depth trend at all locations, and the spatial variation in densification is also evident. At two locations (CMP2 and CMP3 in Fig. 1), densities range from 370-800 kg m^{-3}, with noticeable kinks at approximate depths of 12, 16, 23, and 26 m. We believe that the change in the density trend is possibly due to years with relatively high precipitation and low melt (Fig. 11). However, this trend is not the same at the Jungfraufirn area (CMP4, red line in Fig. 11), with a steady increase of the density starting at approximately 420 kg m^{-3} at about 3 m depth and reaching a maximum density of around 750 kg m^{-3} at 22 m depth.

4.3 Testing and calibration of firn compaction models

The glaciological (direct) and geophysical (indirect, CMP) results provide 1-D firn density distribution data for several balance years. We tested firn compaction models against these results by forcing them with regional climate data from weather stations

https://doi.org/10.5194/egusphere-2025-615
Preprint. Discussion started: 28 March 2025

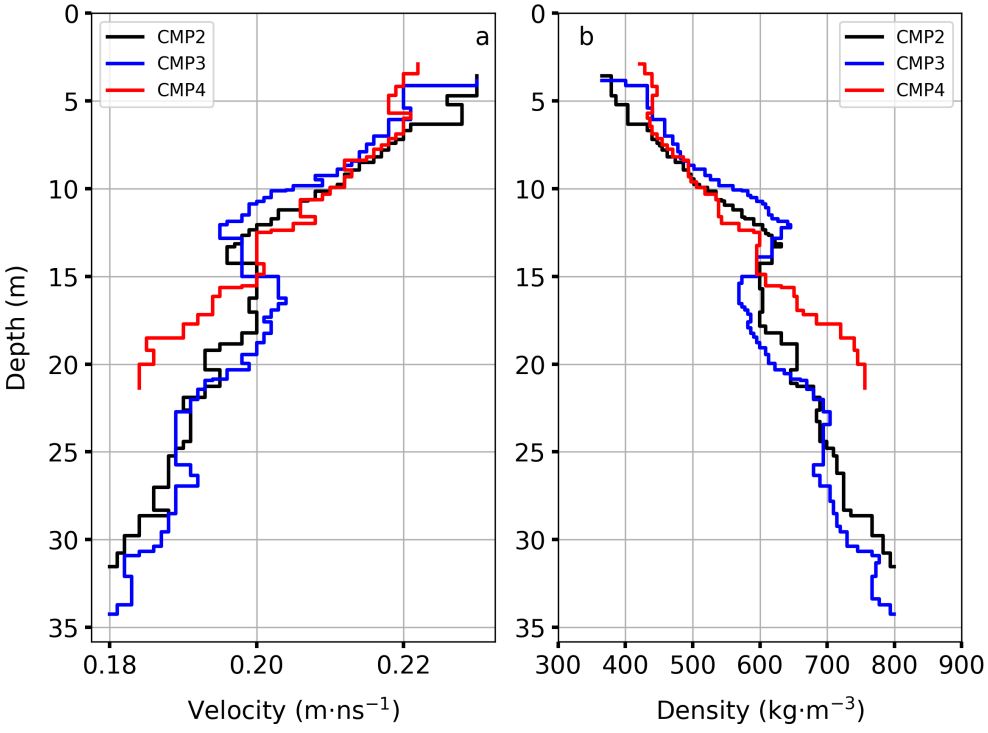

Figure 11. GPR CMP-derived velocity-depth profiles (a) and corresponding density-depth profiles (b) obtained at three accumulation areas of Aletsch glacier. All CMP data were acquired on 16th and 17th May 2024.

and tuning the model coefficients to understand how well the model output represents the observed geophysical and glaciological firn density profiles. The results for the KM and LIG models are illustrated in Figure 12 (a and b) at 3600 and 3400 m a.s.l., representing the Mönchsjoch and Ewigschneefeld locations. It is evident from the model results for Mönchsjoch that density increases with depth. At shallower depths (<8 m), the model density is well below the typical firn density value (450 kg m^{-3}), and there is a shift in the density profile towards higher density below 10 m depth, reaching 550 kg m^{-3} at approximately 12 m depth. Beyond this point, the modelled density profile fluctuates and increases with depth, reaching a pore close-off density (830 kg m^{-3}) at approximately 50 m depth.

We ran the same models at a lower elevation (3400 m a.s.l.), but the results were not significantly different, except for a sharp spike in density at approximately 3 m depth and reaching the pore close-off density (830 kg m^{-3}) beyond 50 m depth. The KM and LIG models exhibit indistinguishable variability at depths <10 m in the density profile, but beyond 10 m depth, model results indicate a minor density offset between each other at the two elevations, despite changes in input parameters such as temperature and melt rate corresponding to the 200 m difference in elevation. It is identifiable that the modelled density profiles better represent the observational (CMP) results at Mönchsjoch than at Ewigschneefeld and Jungfraufirn (near the stake). However, at shallower depths (<8 m), the model density trend is not comparable with the glaciological results.

https://doi.org/10.5194/egusphere-2025-615
Preprint. Discussion started: 28 March 2025

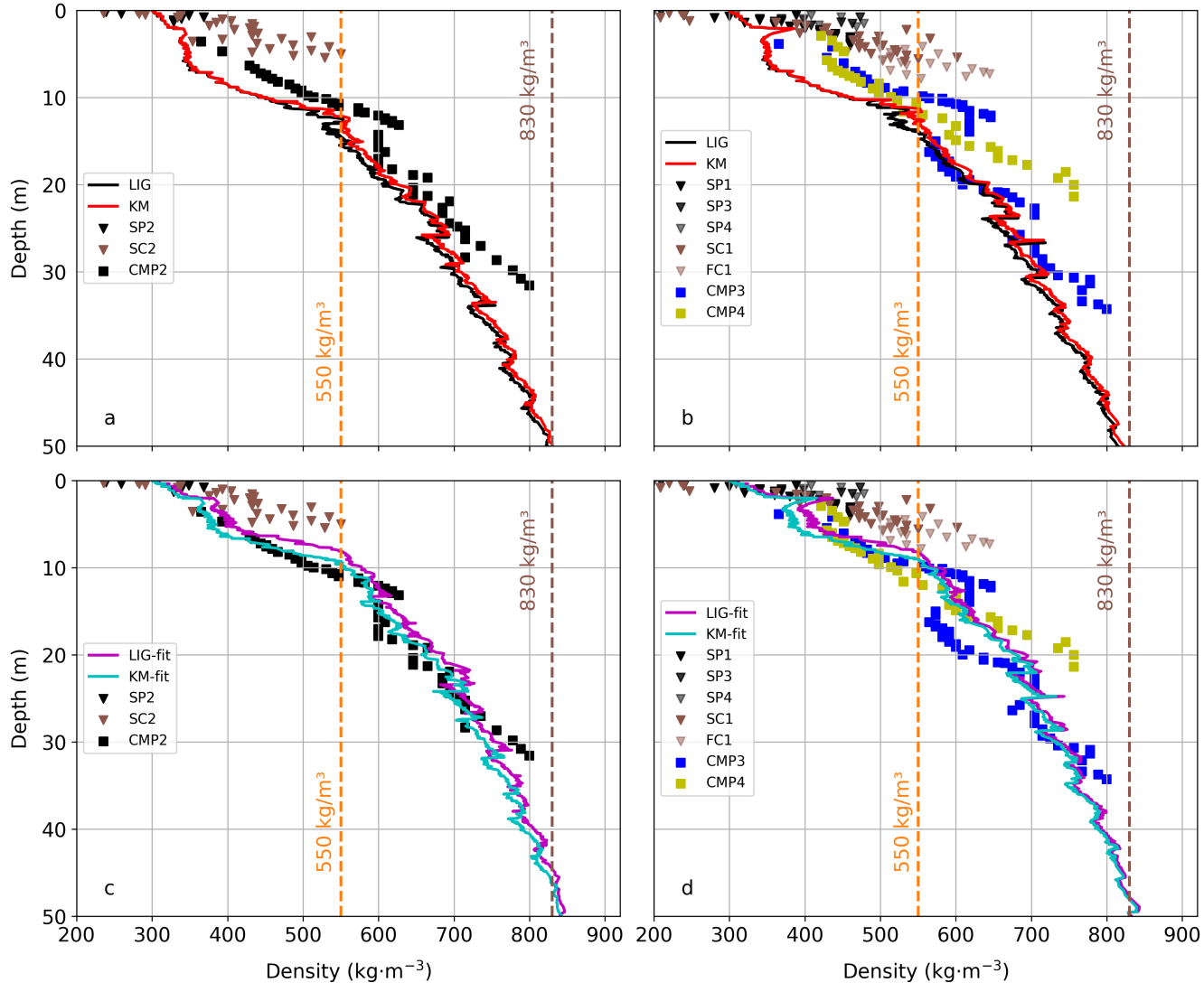

Figure 12. The tested CFM density depth profiles for KM and LIG physics under the regional climate forcings to represent the observational results from snow pits, snow cores and firn core (brown and black arrows) and GPR CMP (black and blue cross) methods obtained during 2024 May measurements are shown here. (a) The KM (red) and LIG (black) model results at Mönchsjoch, (b) Comparing the KM (red) and LIG (black) model at Ewigschneefeld density-depth results with the observations from CMP and snow-pits (SP2, SP3 and SP4, black arrows), snow and firn cores (SC1, SC2 and FC, brown arrows). (c) The tuned KM and LIG model coefficients (cyan and purple, respectively) fit the observational results at Mönchsjoch (3600 m a.s.l). (d) illustrate the similar trend of density profiles from LIG and KM (cyan and purple, respectively) at Ewigschneefeld (3400 m a.s.l). It can also be seen that the depth to firn density > 550 kg m^{-3} (orange dashed line) and pore close-off density (brown dashed line) for CFM and observed results.

When the model coefficients were tuned (Table 2) to fit the observational results at both elevations (Fig. 12 c and d), the

https://doi.org/10.5194/egusphere-2025-615
Preprint. Discussion started: 28 March 2025

results better matched the in-situ observational density profile by shifting the density profile towards higher values, reaching approximately 550 kg m^{-3} at a depth of 10 m, similar to the density trend obtained from CMP analysis at all three locations of the Aletsch glacier. Interestingly, after the tuning, the modelled density results exceed the pore close-off density (830 kg m^{-3}) well before reaching 50 m of depth at Mönchsjoch (45 m) and Ewigschneefeld (49 m). It is observable that, at both elevations and in both tuned and untuned scenarios, the model density trend does not depict the sharp fluctuations at shallower depths (<8 m) matching the glaciological density results. However, the KM and LIG models mimic the in-situ density trend, primarily CMP-derived, at both elevations better than direct observations. The sensitivity tests for three-degree day factors (3.5, 5.5, and 8.5 $°C^{-1}$ day^{-1}) demonstrate similar density trends at both elevations for the LIG and KM models before and after tuning. However, higher factors shift the density profiles towards higher values, reaching the pore close-off density at shallower depths (depth <40 m, Appendix Fig. A1). The effect of the highest value (8.5 $°C^{-1}$ day^{-1}) is more pronounced at Ewigschneefeld compared to Mönchsjoch for the tuned LIG and KM models.

4.4 Tracing the Accumulation history using GPR

The seasonal mass balance estimated from the manually measured snow depth and density from the installed stake at the Jungfraufirn accumulation area of the Aletsch glacier are illustrated in Figure 13. In the last two decades, the lowest winter precipitation was in 2021-22 (approximately 1150 mm w.e.), while the mean winter balance was around 1890 mm w.e., with a maximum of roughly 2860 mm w.e. in 2023-24. The SWE results indicate that the regional interannual precipitation variability fluctuates significantly over short periods. The summer of 2022 was a particularly extreme event within the last two decades, with peak melting of approximately 2060 mm w.e., resulting in the complete loss of the annual firn layer and partial ablation of the 2021 summer layer (Fig. 13) at the Jungfraufirn location. Despite experiencing significant summer melt events in the past eight years, the average summer mass balance over the last 20 years has remained around -450 mm water equivalent (w.e.). This average is maintained due to the occurrence of positive summer balances in specific years, such as 2016, 2014, 2013, 2007, and 2006. The annual SWE measurement (Fig. 13, grey bars) indicates the available yearly firn in mm w.e after the melt season, which helps to interpret radar-derived SWE results to identify IRHs as firn layers, aiding in tracking accumulation history.

Similarly, Figure 14 demonstrates the estimated SWE comparison between all three CMP measurements during the 16-17 May 2024 campaign and the GPR profile obtained at Ewigschneefeld on 29 February 2024, following the analysis in section 3.5. We compared all three CMP-derived SWE estimates with the stake-estimated SWE to validate the IRHs as annual layers. The CMP gathered SWE at the stake (CMP4, from Fig. 16) agrees with the stake-estimated annual SWE, as both were measured nearby. Additionally, the SWE estimated from CMP3 (at Ewigschneefeld) and CMP2 (at Mönchsjoch) correlates well with the stake-estimated annual SWE. However, there is an observable shift in CMP3-measured SWE at Ewigschneefeld and CMP2-derived SWE at Mönchsjoch for older firn layers, yet results are within an acceptable range (R^2 well above 0.8 for both locations). The GPR profile-derived SWE presents palpable variability across periods, which we attribute to uncertainties in considering the mean TWT for SWE estimation (discussed in sect. 6), and the corresponding R^2 is much lower for the GPR-derived SWE comparison (R^2 = 0.65). Due to the strong melt event during the summer of 2022, despite the ablation of the

https://doi.org/10.5194/egusphere-2025-615
Preprint. Discussion started: 28 March 2025

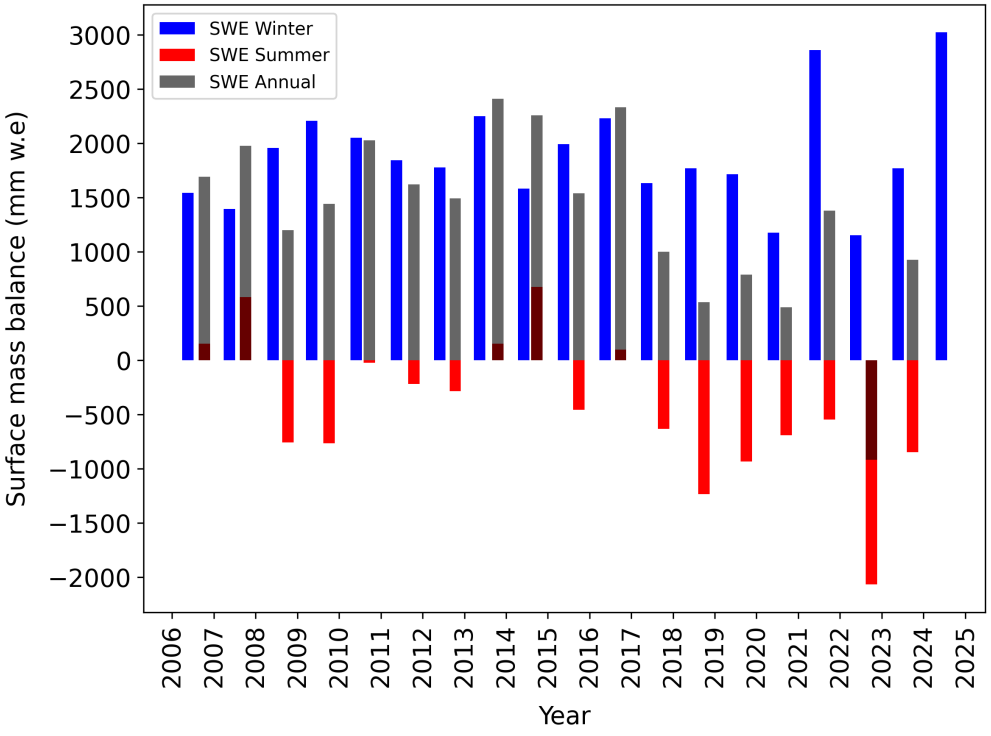

Figure 13. The mass balance of the Aletsch glacier accumulation area measured at the stake near the Jungfraufirn area. The winter (blue) and summer balance (red) on the accumulation area were measured at the end of each season. The annual balance (grey) was estimated by adding the SWE from the winter and summer seasons of the last 20 years. Data provided by Dr Andreas Bauder ETH Zurich Switzerland.

entire layer from the previous season near the stake at Jungfraufirn (Fig. 13), we expect some firn to remain at Mönchsjoch and Ewigschneefeld. The comparison of SWE indicates that a firn layer from the 2022-23 period, measuring approximately 500 mm w.e., remains present across the upper section of the Aletsch glacier. This finding is supported by the observed thinning of IRHs within the GPR transect radargram (Fig. 4). Additionally, Figure 14 reveals that no firn layer is present for the summer of 2022-23 at the CMP4 location. In contrast, the Mönchsjoch and Ewigschneefeld locations show the presence of the firn layer. Moreover, the 2021-22 firn layer is more ablated by approximately 920 mm w.e. at the stake location (Fig. 14, cyan bar), as compared to the CMP2 and CMP3 locations.

4.5 Spatial firn distribution

We traced the spatial distribution of firn density and accumulation along the GPR profile at Ewigschneefeld. Figure 15 shows the firn density within the identified firn layers along the GPR profile. As explained in Section 3.6, density estimates vary from higher elevations (approximately 3550 m a.s.l.) to lower elevations (3380 m a.s.l.) along the GPR profile. It is evident that firn density increases with depth along the transect (approximately 400-800 kg m^{-3}). The influence of elevation change is

https://doi.org/10.5194/egusphere-2025-615
Preprint. Discussion started: 28 March 2025

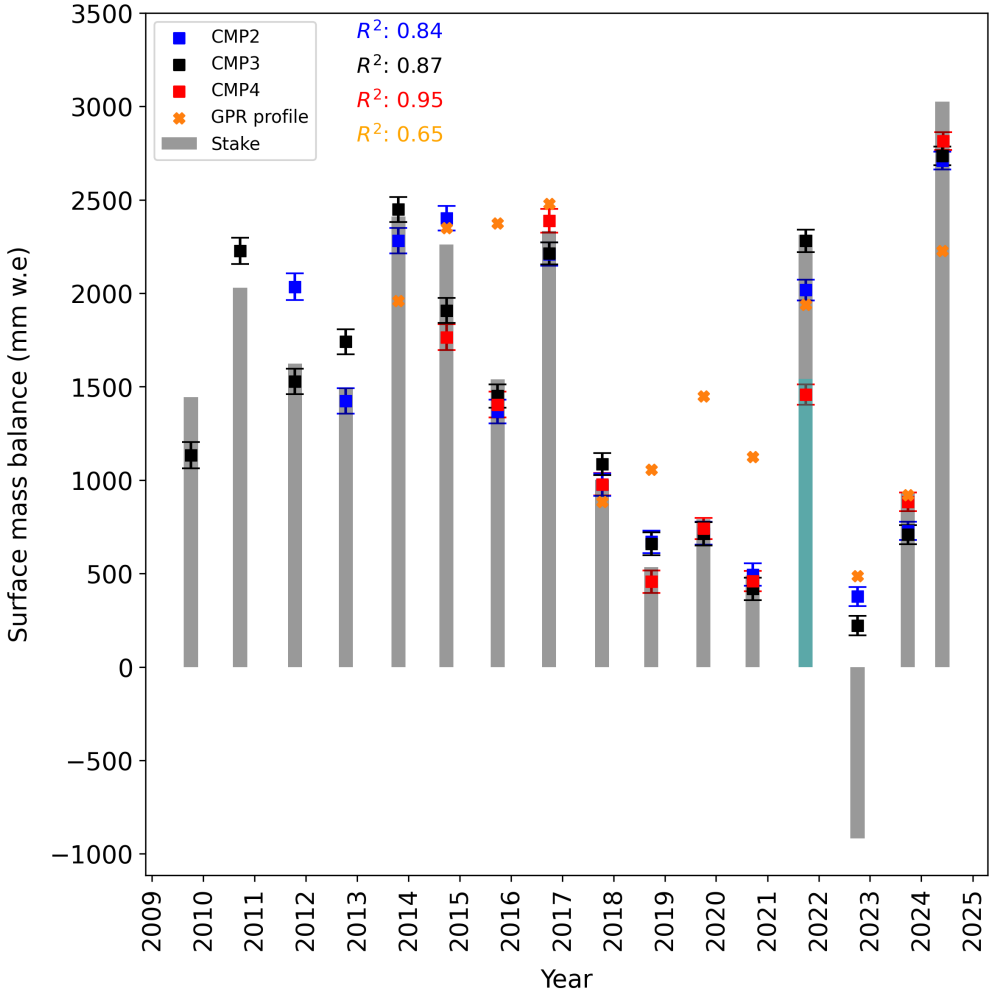

Figure 14. Illustration of identification of IRHs as annual layers and corresponding error analysis due to the uncertainties in IRHs picking in the CMP semblance analysis. Each error bar represents a picking uncertainty of 1 ns resulting in the 43-72 mm. W.e fluctuation in the accumulation. The plot also shows the corresponding R^2 value to fit the stake measured and CMP-derived SWE for all GPR and CMP data gathered during the 2024 expedition. The 2022 summer melt was extremely high with complete ablation of the firn layer at the CMP4 (Stake) location and the further ablation of the 2021 firn layer. The cyan bar in 2021, represents the remainder proportion of the 2021 firn layer after the 2022 summer melt season.

https://doi.org/10.5194/egusphere-2025-615
Preprint. Discussion started: 28 March 2025

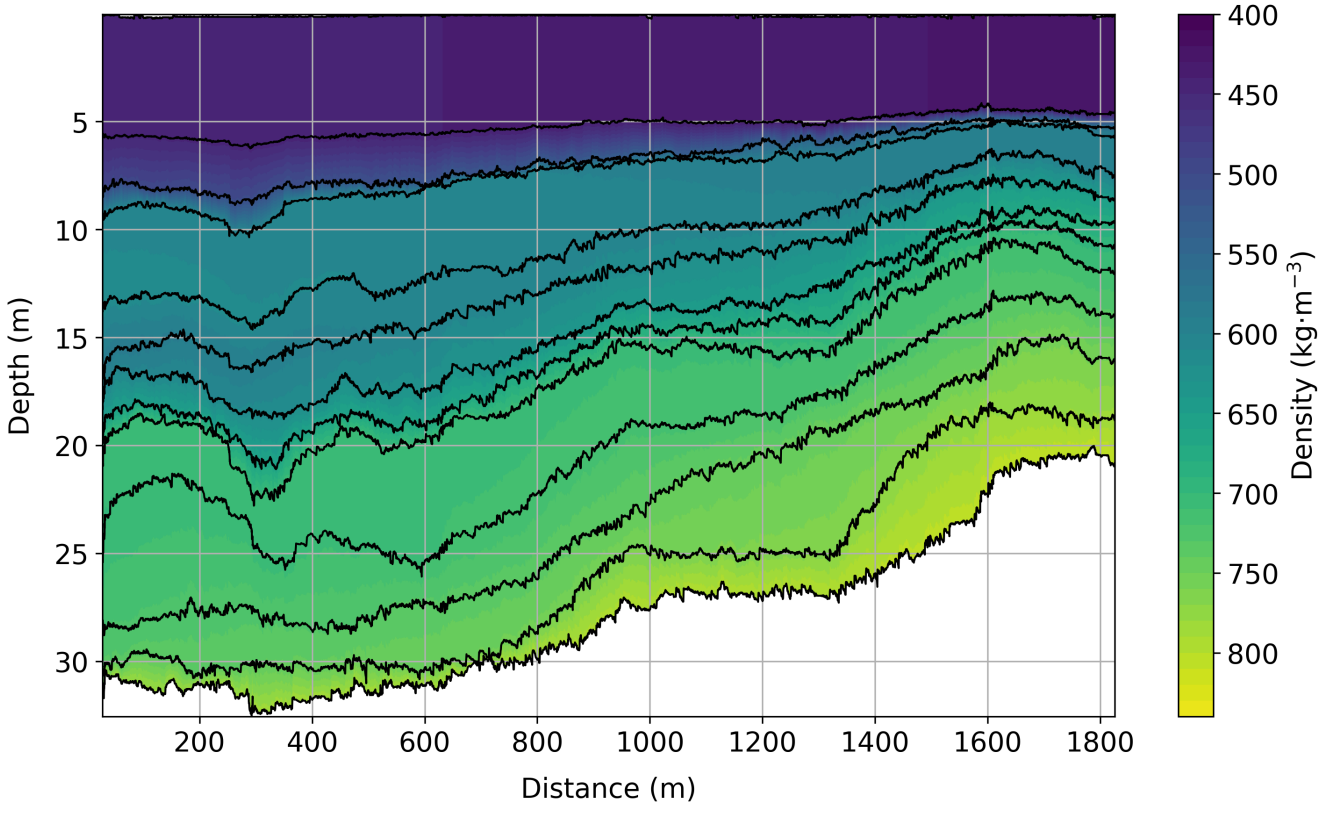

Figure 15. Spatial distribution of firn density along the GPR transect gathered at the Ewigschneefeld. It can be seen that the identified firn layers (black lines) are thinning from higher (3550 m a.s.l) to lower elevation (3380 m a.s.l) along the GPR profile (Fig. 1) represented from left to right.

noticeable, as we move to lower elevations (left to right in Fig. 15), and higher firn density is observed at shallower depths. For instance, the maximum firn density of approximately 780 kg m^{-3} is seen at around 32 m (left), but the same density appears at a depth of approximately 21 m at the lower end of the GPR profile (Fig. 15, right side).

Spatial variation in estimated SWE along the same GPR profile is illustrated in Figure 16, which represents the accumulation within identified annual layers. As the density within each layer varies along the GPR profile, the estimated SWE within each layer changes due to variations in layer thickness and density. This also demonstrates the spatial variability in the accumulation history, indicating that in the upper part of the GPR profile, the SWE is higher due to thicker firn layers, suggesting higher precipitation and lower melt. As we move downward along the profile, firn layer thickness reduces, leading to lower accumulation as elevation decreases. We can also observe that the 2024 winter precipitation above the last summer horizon (0-5 m depth) mostly remained constant along the profile (>1800 mm w.e). However, as depth increases, the thickness of identified annual firn layers reduces with decreasing elevation along the profile (left to right in Fig. 16). Notably, thicker firn layers have higher

https://doi.org/10.5194/egusphere-2025-615
Preprint. Discussion started: 28 March 2025

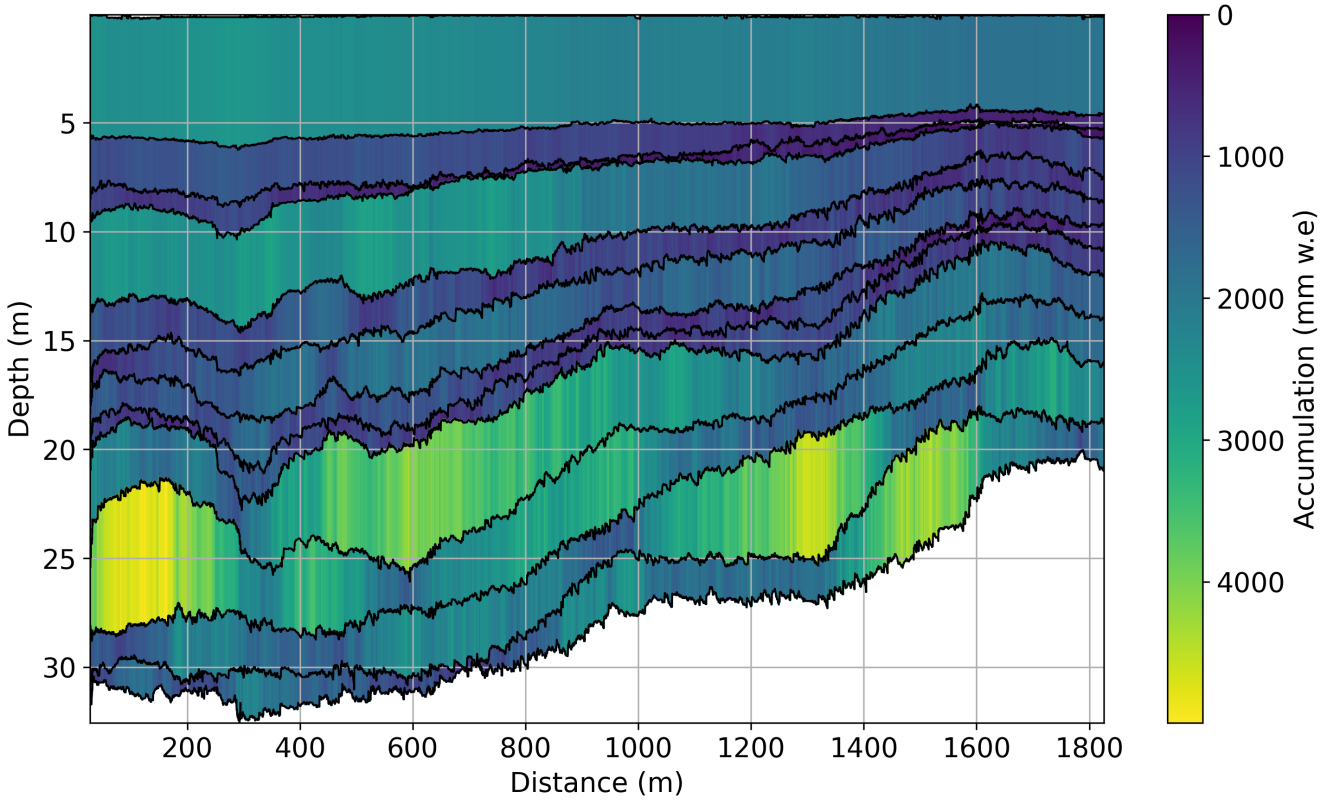

Figure 16. Spatial accumulation distribution within firn layers along the GPR transect gathered at the Ewigschneefeld. Accumulation varies within identified firn layers (black lines) as the thickness and density vary along the GPR transect from higher to lower elevation (3550 m a.s.l on left to 3380 m a.s.l on right).

accumulation (>4200 mm w.e) at deeper depths (e.g., depths between 22-28 m), attributed to denser firn layers as shown in Figure 15.

5 Discussion

5.1 Local firn density profiles using GPR

We investigated the last summer horizon, as well as the firn structure and density profiles up to 7.8 m at the Ewigschneefeld and 5.4 m at the Mönchsjoch with glaciological methods, covering a 2023 firn layer starting approximately at 4.8-5 m depth (Fig. 8). Identified cluster of ice lenses (depth < 4.8 m) within snow and firn cores hints at refrozen meltwater complemented by the results from isotope analysis (Fig. 9). The glaciological results from both locations show a similar density structure except for the offset of nearly 100 kg m^{-3} in the upper first meter. We believe that the extreme weather, characterized by high wind and

https://doi.org/10.5194/egusphere-2025-615
Preprint. Discussion started: 28 March 2025

precipitation during the two-day gap between snow cores (SC1 and SC2), caused the surface snow density offset. Due to these weather conditions, we could not gather any data near the stake (Jungfraufirn in Fig. 1) in March 2024. The estimated winter accumulation at Ewigschneefeld is approximately 2700 mm w.e., based on the combined measurements from SP1, FC1 (depth up to 5 m) and SP3 (Fig 1). The stake-measured accumulation at Jungfraufirn for the same period is around 3000 mm w.e., which results in an offset of about 300 mm w.e. We assume this discrepancy arises for two reasons. First, we could not reach the surface of SP1 when we dug a shallow snowpit (SP3) on 17 May 2024. Second, the spatial variability between SP1, SP3 and Stake at Jungfraufirn (Fig. 1), along with possible precipitation events between 17 May and 6 June 2024, likely contributed to the higher total winter accumulation.

The glaciological approach only provides point-scale results, which are limited to a shallow depth. For this reason, our investigation using geophysical means (GPR) helps to understand the firn structure and density profiles down to larger depths (>30 m). The results of the firn structure and 1-D firn density profiles derived from GPR CMP data provide a detailed understanding of the density distribution at different locations of the accumulation area of the Aletsch glacier. Our investigation shows similar density profiles at Mönchsjoch and Ewigschneefeld (CMP2 and CMP3 in Fig. 11). The significant density changes at depths of 12, 16, and 23 m are likely due to the positive summer balances in 2016, 2014, and 2013, which had higher winter precipitation and lower summer melt (Fig. 13). The colder conditions during these years very likely resulted in less melting, causing the observed density variations at these depths.

The radar penetration depth varies at all three locations, indicating that the attenuation of radar energy differs. The significant attenuation reducing radar penetration to less than 22 m at CMP4 (Fig. 11) is likely due to changes in the dielectric and conductivity properties of the subsurface (Davis and Annan, 1989). Zhao et al. (2016) show increased radar wave attenuation attributed to the presence of liquid water, which is evident in temperate glaciers during summer. We attribute the reduced penetration depth at the CMP4 location (Fig. 11) to the effect of melt and refreezing at lower elevations, leading to reduced radar penetration depth compared to the other CMP locations (CMP2 and CMP4 in Fig. 11). Using GPR to derive firn density profiles is not a new approach. For instance, Brown et al. (2012) demonstrated the effectiveness of CMP georadar surveys in estimating density variations within the firn column at 13 locations along the Expédition Glaciologique Internationale au Groenland (EGIG), covering the percolation area of the Greenland ice sheet (GrIS). However, we found no studies focusing on GPR-derived firn density estimations in alpine glacier conditions. While Brown et al. (2012) validated their method by comparing it with deep firn core data (up to 120 m), we lack such comprehensive firn core data in our research. Additionally, we used a commonly employed semblance analysis method to analyze the CMP data, as opposed to the travel time inversion method described by Zelt and Smith (1992) and used in Brown et al. (2012).

5.2 Modelled firn densification

Many studies have developed firn compaction models and validated existing ones through direct physical observations, such as those by Herron and Langway (1980); Arthern et al. (2010); Ligtenberg et al. (2011). As mentioned earlier, all these models were tested and calibrated for polar conditions. However, studies like Huss (2013) used a modified version of the Herron and Langway (1980) firn densification model for temperate glaciers. The employed firn compaction model was calibrated using

https://doi.org/10.5194/egusphere-2025-615
Preprint. Discussion started: 28 March 2025

density measurements from 19 firn cores across various mountain glaciers and ice caps. Similarly, Sold et al. (2015) applied Reeh (2008) firn layer compaction model, which is also based on the classical Herron and Langway (1980), assuming a linear relationship between firn densification and overburden snow or firn pressure over time. This study calibrates the model with a scaling factor that depends on the measured and modelled IRH travel times. We demonstrate the use of LIG and KM models from the CFM modular run, forced with temperate glacier climatic conditions, to primarily represent geophysical observations. Later, the models were tuned to fit the CMP-derived density-depth trend (Sect 3.3.1).

Figure 12 shows the 1-D firn densification after forcing the LIG and KM models with regional climate inputs and evaluating them against the locally obtained firn density profiles from glaciological and geophysical methods at two elevations. We observed that both models behave similarly at both elevations, implying no noticeable impact from small variations in temperature and melt rate settings. When the CFMs were not tuned, the model results showed an offset from the glaciological observations at lower depths (<8 m), leading to an underestimation of shallow firn density. However, when we tuned the CFMs to fit the CMP-derived firn density profiles, the offset at shallower depths disappeared. The sensitivity analysis of CFM models to the melt rate revealed no significant changes in the upper firn densification, except for a spike in density at 4 m depth (Fig. A1 in the appendix). In our study, we did not focus on the details of firn physical processes such as grain growth, water retention, and permeability. Instead, we aimed to test the models' ability to represent geophysically derived in-situ firn densification results. This was achieved solely by tuning parameter coefficients (Table 2) without changing the physics or empirical equations of the CFM. However, the tested LIG and KM models consider temperature, accumulation, liquid water percolation and refreezing in vertical 1-D firn compaction (Ligtenberg et al., 2011). Our CFM results agree rather well with the CMP-derived firn densification profile, encouraging further development of firn compaction models in temperate conditions, combined with geophysical observations, to obtain enhanced information on firn density and its evolution.

5.3 Sensitivity of field results

The GPR and CMP analyses not only provide the radar wave velocity profile within the firn but also estimate the IRH depths. However, the semblance analysis used to extract the radar wave propagation velocity has uncertainties associated with picking the semblance wave peak, mainly at shallow IRHs, resulting in velocity measurement errors (Murray et al., 2007). According to Frolov and Macheret (1999), the velocity of radar waves depends solely on the relative permittivity of the medium. It is also quantified that 3% water content would reduce the velocity by 0.03 m ns^{-1} within the snowpack. Since we collected the CMP data at the end of winter when temperatures were well below freezing, we can ignore the effect of meltwater and assume a two-phase firn system (ice and air) for radar velocity, as explained in Bradford et al. (2009). However, the manual picking of the IRH and velocities is also affected by subjective errors.

We estimated that a velocity picking uncertainty of 0.005 m ns^{-1} results in a ~ 36 kg m^{-3} variation in density (Eq. 1). Additionally, an IRH depth sensitivity of 1 ns with no change in velocity could result in ~ 45 mm w.e. variation in SWE estimation. Figure 14 illustrates the error analysis for estimating SWE within the identified firn layer. The analysis shows that an uncertainty of 1 ns in picking affects depth, radar velocity, and density estimation, which can cause SWE to vary between 40 and 75 mm w.e. The SWE error is amplified when we choose the mean TWT for the identified firn layer from the GPR profile (orange

https://doi.org/10.5194/egusphere-2025-615
Preprint. Discussion started: 28 March 2025

cross in Fig. 14) obtained at the Ewigschneefeld. The firn layers seen on the radargram show that the IRH thickness reduces as we move downhill along the profile (left to right in Fig. 2). Thus, the picked firn layer can vary by up to 100 ns from one end to another (e.g., from ~186 ns to ~108 ns in Fig. 2). As we select deeper firn layers, the variation in firn layer depth along the profile from one end to the other increases (e.g., from approximately 311 ns to 174 ns). Therefore, it is practical to use the mean TWT to estimate SWE along the GPR transect for the identification of the annual firn layer.

5.4 Accumulation history and spatial firn distribution

In addition to the local firn density profiles at three locations in the accumulation area of the Aletsch glacier, we estimated the depth of the annual firn layers from the CMP-derived velocity-depth profile. As stated earlier, we identified the many IRHs within the CMP data, and it should be noted that not all IRHs necessarily represent annual firn layers. Therefore, to identify the IRHs as annual layers, we introduced an iterative method by estimating the SWE between each IRH and validating it against the physically observed SWE from the stake measurements available at the Jungfraufirn (near the stake, Fig. 1). The CMP4 measurements are close to the stake observation, making it reliable to match the yearly SWE, which is evident from the high correlation (R^2 = 0.95). The CMP2 and CMP3 comparisons show lower correlation (R^2 = 0.84 and 0.87) due to the spatial variability in the firn distribution.

We assessed the role of extreme events, such as high melt during the summer of 2022, on the detection of firn layers before and after this event (2023 and 2021). As already explained, the complete ablation of the 2022 seasonal layer (~2000 mm w.e) complicates the identification of firn layers from the IRHs detected at deeper depths. At the Jungfraufirn location, the 2022 firn layer does not exist (Fig. 13), but this might not be true for Mönchsjoch and Ewigschneefeld. This argument is supported by the radargram obtained from the GPR profile at Ewigschneefeld, demonstrating the strong IRH (at 140 ns in Fig. 2) that persists with a certain thickness in the upper part of the GPR transect and vanishes as the profile reaches lower elevation. Furthermore, Mönchsjoch (CMP2) and Ewigschneefeld (CMP3) are situated at higher elevations than CMP4 (Stake) (Fig. 1), providing evidence for the survival of the 2022 firn layer. Abundantly identified IRHs at deeper depths beyond the 2022 layer (depth >120 ns in Fig. 2) reflected in CMP data potentially resulted from refrozen meltwater during the 2022 melt season event. To classify IRHs as annual firn layers, the iterative method helps in choosing IRHs chronologically and then estimating the SWE that fits the stake-estimated results (Fig. 12).

A main difference between our study and that of Sold et al., 2015 at Findelengletscher is the usage of the CMP method, which provides a solid estimation of depth to the IRHs, covering deeper firn layers. The study by Sold et al., 2015 relied on the GPR travel time of each layer compared with the firn compaction model for firn densification. To translate the IRH travel time to depth, the Sold et al., 2015 study depends on the relationship between firn density and dielectric permittivity of firn (Frolov and Macheret, 1999). The study also relies on firn core data and repeat GPR measurements over consecutive years. In contrast, we extract the firn density-depth profile solely from the GPR CMP method without relying on firn core data and model results. However, misinterpretation of IRH affects the SWE estimation, which in turn alters the chronology of the annual firn layer by shifting the deeper layers. Therefore, the iterative method of matching the GPR-derived SWE with the stake-derived SWE helps to avoid misinterpretation. We traced up to 15 years of firn layers (Fig. 14) and estimated the SWE of each layer at three

https://doi.org/10.5194/egusphere-2025-615
Preprint. Discussion started: 28 March 2025

accumulation areas. However, CMP-derived accumulation history is constrained to point information, similar to firn cores and stake measurements. We addressed this issue by measuring the GPR transect at Ewigschneefeld (Fig. 1) and identified more than 10 prominent IRHs down to a depth of more than 30 m. The radargram shows distinctive and continuous firn stratigraphy along the profile. It should be noted that most IRHs run almost parallel to each other and thin towards lower elevations. This provides vital information about the spatial variability in the accumulation history and the melt rate.

The main drawback of our analysis with the firn layer identification from the GPR profile is the availability of just one CMP dataset (CMP3 in Fig. 1) on the uppermost part of the transect. The lack of CMP data at the lower part forced us to assume the IRHs as straight lines to estimate SWE within each layer by considering the mean TWT of each IRH. The resulting firn layer SWE roughly correlates with the stake-measured SWE ($R^2 = 0.64$). The deeper firn layers (>200 ns in Fig. 1) show a dip in the IRHs and some discontinuities, which we speculate as effects of glacier dynamics causing the undulations. However, tracking the spatial firn distribution within the identified firn layers is possible by extending the density-depth profile from 7.8 m to 34.8 m (Sect. 3.6, Fig. 7) at the far end of the GPR transect. The shift in the density profile when compared with the CMP-derived density profile signifies the effect of reduced elevation on firn densification.

The spatial firn distribution presented in this study (Fig. 15 and 16) relies on CMP data to determine the average velocity above the reflector's depth. This approach assists in estimating the density and accumulation distribution across the spatial scale. The observed changes in firn stratigraphy reveal variations in accumulation history, as demonstrated by the spatial accumulation distribution (Fig. 16). This finding is supported by the Bannwart et al., 2024 study, which shows similar firn stratigraphy from a winter 2021 GPR transect at the same location as our measurements. However, the deeper firn layers in the lower part of our GPR transect exhibit unacceptably high accumulation (at distance > 1000 m and depth > 20 m in Fig. 16). We attribute this to potential uncertainties in semi-automatic picking of IRHs using the phase-follower in ReflexW software due to lack of the visibility of IRHs at that location. To enhance the analysis, we recommend conducting more than one CMP measurement if the GPR profile indicates significant variations in firn stratigraphy along the transect. Our study heavily depends on long-term manual accumulation stake measurements at Jungfraufirn to derive accumulation history and firn distribution. The spatial variability of accumulation within each layer is likely influenced by variable precipitation distribution linked to elevation differences and temperature lapse rates, causing significant melt at the lower end of the GPR profile.

The primary takeaways from our study include the application of the CMP method in temperate conditions to derive firn density-depth profiles in accumulation area, and an introduction of an iterative approach that relies on stake-derived SWE to validate the IRHs as annual layers. Consequently, this approach aids in tracing the spatial firn density and accumulation history. Moreover, the focus of firn compaction modelling is to represent in-situ results. The combination of GPR (including CMP) and the firn compaction modelling approach defines the geometry and internal structure of the firn body. Our results show the potential to track the pore close-off depth (firn to ice transition) by tuning the firn compaction models with the CMP-derived density profiles. We believe that the non-invasive approach of GPR-derived density profiles helps calibrate the firn densification models, unlike other studies that rely on laborious in-situ glaciological observations. Our study demonstrates the importance of integrating in-situ geophysical, glaciological methods and firn densification modelling to understand the evolution of firn

https://doi.org/10.5194/egusphere-2025-615
Preprint. Discussion started: 28 March 2025

structure and density. Such an approach is a significant step toward improving the uncertainties in density assumptions in geodetically derived glacier volume-to-mass estimates, where firn density consideration is limited.

6 Conclusions

By utilizing geophysical methods, we introduced a novel approach to acquiring firn structure, density, and accumulation history distribution on both local and spatial scales in the accumulation area of the Aletsch glacier. Our method relies on radar wave propagation velocity to accurately estimate the depths to the IRHs and trace firn density profiles in various parts of the accumulation area. Additionally, we tested the firn compaction models (CFM) under regional climate forcing and tuned the model's coefficients to best match the in-situ results. In the next step, the models themselves could be adapted to better represent the firn structure for alpine conditions. This highlights the significance of these models in predicting firn density evolution in future studies, particularly in the absence of field data.

We demonstrated that glaciological methods helped to identify the last summer horizon and thus support the interpretation of the indirect GPR measurements. By coupling the estimated SWE from manual stake measurements with the CMP-derived SWE, we classified the IRHs as annual layers and distinguished the last 15 years' firn layers on a local scale at three accumulation areas of the glacier. Like other studies, our results are not exempt from limitations and uncertainties, particularly in interpreting the IRHs as annual layers. To address these uncertainties, we suggest including at least one deep firn core (depth >15 m) covering more than two annual layers near the CMP location in future studies for the accurate interpretation of the IRHs as annual firn layers. We demonstrated the intercomparison of firn structure, density, and accumulation history through geophysical, glaciological, and modelling approaches.

The information content of GPR profiles along the firn basins is strongly improved by using the CMP method in tracking the density profile and by the additional accumulation history derived from the annual firn layers linked with the stake-derived seasonal SWE. We recommend using GPR during winter, especially in temperate glacier conditions, as it provides deeper penetration depths and helps identify more firn layers. This combined approach allows us to derive the accumulation history over a larger spatial scale, mitigating the limitations of traditional firn core methods in challenging alpine conditions. Our investigations also demonstrate the possibility of mapping entire firn bodies by the combined methods and thus characterising the density contribution of the accumulation zones to the mean glacier density.

Appendix A

https://doi.org/10.5194/egusphere-2025-615
Preprint. Discussion started: 28 March 2025

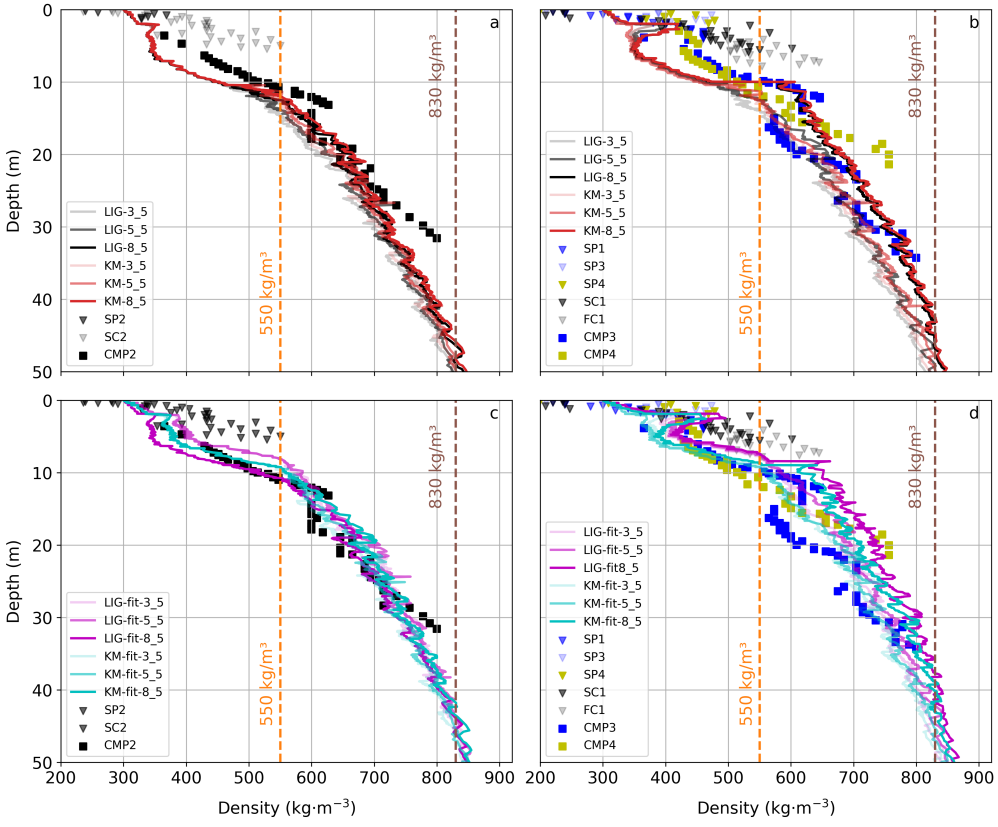

Figure A1. Sensitivity analysis of the LIG and KM CFM models for different melt rates. Model's density profiles at the Mönchsjoch (a) and Ewigschneefeld (b) for the three different degree day factors of 3.5, 5.5 and 8.5 mm $^{\circ}C^{-1}$ day^{-1} compared with the respective in-situ results (Fig. 1). The density profiles after tuning the LIG and KM models (c and d) at both locations to fit for the observational results. Here models were tuned for the same parameter coefficients but changing the melt rates.

https://doi.org/10.5194/egusphere-2025-615
Preprint. Discussion started: 28 March 2025

Data availability. The raw data acquired during the 2023-24 expeditions are available from the BAdW LRZ online repository. Processed data can be obtained upon request. We plan to publish the dataset, creating a DOI that includes both raw and processed data. The DOI will be available upon the acceptance of the manuscript.

Author contributions. A.P., with assistance from C.M., initiated and developed the study. A.P. wrote the paper and conducted the data analysis. The field campaigns were planned with contributions from C.M., T.S., and A.G. T.S. and A.G. analyzed the firn core, snow core, and snow pit data from the February-March 2024 campaign, while C.M. analyzed the snow pit data from the May 2024 fieldwork. All co-authors contributed to the reviewing and editing of the manuscript.

Competing interests. The authors declare that they have no conflict of interest

Acknowledgements. The study was funded by the Bavarian State Ministry of Science and the Arts within the Elitenetwork Bavaria International Doctoral Programme “MOCCA - Measuring and Modelling Mountain Glaciers and Ice Caps in a Changing Climate”. We would like to thank the following colleagues for their support during the expeditions in the accumulation area of the Aletsch glacier in February-March 2024 and May 2024: Astrid Lambrecht, Felix Pfluger, Patricia Schlenk, Manuel Saigger, and Michael Stelzig. We also acknowledge the data from Dr. Andreas Bauder from ETH Zurich and we appreciate Dr. C. Max Stevens from the University of Maryland for assisting us in understanding the application of the Community Firn Model (CFM) in our study. We also thank the International Foundation High Alpine Research Stations Jungfraujoch and Gornergrat (HFSJG), the Jungfraujochbahn for the smooth conduction of our expeditions.

https://doi.org/10.5194/egusphere-2025-615
Preprint. Discussion started: 28 March 2025

References

Aizen, V. B., Aizen, E., Fujita, K., Nikitin, S. A., Kreutz, K. J., and Takeuchi, L. N.: Stable-isotope time series and precipitation origin from firn-core and snow samples, Altai glaciers, Siberia, Journal of Glaciology, 51, 637–654, https://doi.org/10.3189/172756505781829034, 2005.

Annan, A. P.: Practical Processing of GPR Data, in: Proceedings of the Second Government Workshop on Ground Penetrating Radar, Columbus, Ohio, 1993.

Annan, A. P.: Ground-Penetrating Radar, in: Investigations in Geophysics, pp. 357–438, https://doi.org/10.1190/1.9781560801719.ch11, 2005.

Arcone, S. A. and Kreutz, K. J.: GPR Reflection Profiles of Clark and Commonwealth Glaciers, Dry Valleys, Antarctica, Annals of Glaciology, 50, 121–129, http://www.ingentaconnect.com/content/igsoc/agl/2009/00000050/00000051/art00017, 2009.

Arthern, R. and Wingham, D.: The Natural Fluctuations of Firn Densification and Their Effect on the Geodetic Determination of Ice Sheet Mass Balance, Climatic Change, 40, 605–624, https://doi.org/10.1023/A:1005320713306, 1998.

Arthern, R. J., Vaughan, D. G., Rankin, A. M., Mulvaney, R., and Thomas, E. R.: In situ measurements of Antarctic snow compaction compared with predictions of models, Journal of Geophysical Research: Earth Surface, 115, 2009JF001 306, https://doi.org/10.1029/2009JF001306, 2010.

Bannwart, J., Piermattei, L., Dussaillant, I., Krieger, L., Floricioiu, D., Berthier, E., Roeoesli, C., Machguth, H., and Zemp, M.: Elevation bias due to penetration of spaceborne radar signal on Grosser Aletschgletscher, Switzerland, Journal of Glaciology, pp. 1–15, https://doi.org/10.1017/jog.2024.37, 2024.

Barry, R. G.: The status of research on glaciers and global glacier recession: a review, Progress in Physical Geography: Earth and Environment, 30, 285–306, https://doi.org/10.1191/0309133306pp478ra, 2006.

Bauder, A., Funk, M., and Huss, M.: Ice-volume changes of selected glaciers in the Swiss Alps since the end of the 19th century, Annals of Glaciology, 46, 145–149, https://doi.org/10.3189/172756407782871701, 2007.

Bauder, A., Mazzotti, G., Berger, C., Langhammer, L., Griessinger, N., and Jonas, T.: Winter Accumulation Measurements on Alpine Glaciers using Ground Penetrating Radar, in: 2018 17th International Conference on Ground Penetrating Radar (GPR), pp. 1–5, IEEE, Rapperswil, ISBN 978-1-5386-5777-5, https://doi.org/10.1109/ICGPR.2018.8441559, 2018.

Bender, M., Sowers, T., and Brook, E.: Gases in ice cores, Proceedings of the National Academy of Sciences, 94, 8343–8349, https://doi.org/10.1073/pnas.94.16.8343, 1997.

Benson, C.: Stratigraphic Studies in the Snow and Firn of the Greenland Ice Sheet., Tech. Rep. 70, 1996.

Blunier, T. and Schwander, J.: Gas enclosure in ice: age difference and fractionation, in: Physics of Ice Core Records, pp. 307–326, Hokkaido University Press, 2000.

Bolch, T., Sandberg Sørensen, L., Simonsen, S. B., Mölg, N., Machguth, H., Rastner, P., and Paul, F.: Mass loss of Greenland's glaciers and ice caps 2003–2008 revealed from ICESat laser altimetry data, Geophysical Research Letters, 40, 875–881, https://doi.org/10.1002/grl.50270, 2013.

Bradford, J. H., Harper, J. T., and Brown, J.: Complex dielectric permittivity measurements from ground-penetrating radar data to estimate snow liquid water content in the pendular regime, Water Resources Research, 45, W08 403, https://doi.org/10.1029/2008WR007341, 2009.

https://doi.org/10.5194/egusphere-2025-615
Preprint. Discussion started: 28 March 2025

Brown, J., Harper, J., Pfeffer, W. T., Humphrey, N., and Bradford, J.: High-resolution study of layering within the percolation and soaked facies of the Greenland ice sheet, Annals of Glaciology, 52, 35–42, https://doi.org/10.3189/172756411799096286, 2011.

Brown, J., Bradford, J., Harper, J., Pfeffer, W. T., Humphrey, N., and Mosley-Thompson, E.: Georadar-derived estimates of firn density in the percolation zone, western Greenland ice sheet, Journal of Geophysical Research: Earth Surface, 117, 2011JF002089, https://doi.org/10.1029/2011JF002089, 2012.

Cuffey, K. M. and Paterson, W. S. B.: The Physics of Glaciers, Butterworth-Heinemann, Oxford, 4 edn., 2010.

Cullen, N. J. and Conway, J. P.: A 22 month record of surface meteorology and energy balance from the ablation zone of Brewster Glacier, New Zealand, Journal of Glaciology, 61, 931–946, https://doi.org/10.3189/2015JoG15J004, 2015.

Davis, J. L. and Annan, A. P.: GROUND-PENETRATING RADAR FOR HIGH-RESOLUTION MAPPING OF SOIL AND ROCK STRATIGRAPHY[1], Geophysical Prospecting, 37, 531–551, https://doi.org/10.1111/j.1365-2478.1989.tb02221.x, 1989.

Dunse, T., Eisen, O., Helm, V., Rack, W., Steinhage, D., and Parry, V.: Characteristics and small-scale variability of GPR signals and their relation to snow accumulation in Greenland's percolation zone, Journal of Glaciology, 54, 333–342, https://doi.org/10.3189/002214308784886207, 2008.

Eisen, O., Frezzotti, M., Genthon, C., Isaksson, E., Magand, O., Van Den Broeke, M. R., Dixon, D. A., Ekaykin, A., Holmlund, P., Kameda, T., Karlöf, L., Kaspari, S., Lipenkov, V. Y., Oerter, H., Takahashi, S., and Vaughan, D. G.: Ground-based measurements of spatial and temporal variability of snow accumulation in East Antarctica, Reviews of Geophysics, 46, 2006RG000218, https://doi.org/10.1029/2006RG000218, 2008.

Endres, A. L., Murray, T., Booth, A. D., and West, L. J.: A new framework for estimating englacial water content and pore geometry using combined radar and seismic wave velocities, Geophysical Research Letters, 36, 2008GL036876, https://doi.org/10.1029/2008GL036876, 2009.

Farinotti, D., Huss, M., Bauder, A., and Funk, M.: An estimate of the glacier ice volume in the Swiss Alps, Global and Planetary Change, 68, 225–231, https://doi.org/10.1016/j.gloplacha.2009.05.004, 2009.

Fisher, S. C., Stewart, R. R., and Jol, H.: Processing ground penetrating radar (GPR) data, CREWES Res. Rep, 4, 1–21, 1992.

Fisher, S. C., Stewart, R. R., and Jol, H. M.: Ground Penetrating Radar (GPR) data enhancement using seismic techniques, Journal of Environmental and Engineering Geophysics, 1, 89–96, https://doi.org/10.4133/JEEG1.2.89, 1996.

Frolov, A. D. and Macheret, Y. Y.: On dielectric properties of dry and wet snow, Hydrological Processes, 13, 1755–1760, 1999.

Gagliardini, O. and Meyssonnier, J.: Flow simulation of a firn-covered cold glacier, Annals of Glaciology, 24, 242–248, https://doi.org/10.3189/S0260305500012246, 1997.

Gardelle, J., Berthier, E., and Arnaud, Y.: Impact of resolution and radar penetration on glacier elevation changes computed from DEM differencing, Journal of Glaciology, 58, 419–422, https://doi.org/10.3189/2012JoG11J175, 2012.

GLAMOS: The Swiss Glaciers 1880-2016/17, Glaciological Reports No 1-140, Yearbooks of the Cryospheric Commission of the Swiss Academy of Sciences (SCNAT), Zurich, https://doi.org/10.18752/glrep_series, since 1964 by VAW / ETH Zurich, ed., 2018.

Haeberli, W.: Climate Change and its Impacts on Glaciers and Permafrost in the Alps, 27, 258–265, 1998.

Heilig, A., Eisen, O., Schneebeli, M., MacFerrin, M., Stevens, C. M., Vandecrux, B., and Steffen, K.: Relating regional and point measurements of accumulation in southwest Greenland, The Cryosphere, 14, 385–402, https://doi.org/10.5194/tc-14-385-2020, 2020.

Helm, V., Rack, W., Cullen, R., Nienow, P., Mair, D., Parry, V., and Wingham, D. J.: Winter accumulation in the percolation zone of Greenland measured by airborne radar altimeter, Geophysical Research Letters, 34, 2006GL029185, https://doi.org/10.1029/2006GL029185, 2007.

https://doi.org/10.5194/egusphere-2025-615
Preprint. Discussion started: 28 March 2025

Helm, V., Humbert, A., and Miller, H.: Elevation and elevation change of Greenland and Antarctica derived from CryoSat-2, The Cryosphere, 8, 1539–1559, https://doi.org/10.5194/tc-8-1539-2014, 2014.

Hempel, L., Thyssen, F., Gundestrup, N., Clausen, H. B., and Miller, H.: A comparison of radio-echo sounding data and electrical conductivity of the GRIP ice core, Journal of Glaciology, 46, 369–374, https://doi.org/10.3189/172756500781833070, 2000.

Herron, M. M. and Langway, C. C.: Firn Densification: An Empirical Model, Journal of Glaciology, 25, 373–385, https://doi.org/10.3189/S0022143000015239, 1980.

Hock, R.: Temperature index melt modelling in mountain areas, Journal of Hydrology, 282, 104–115, https://doi.org/10.1016/S0022-1694(03)00257-9, 2003.

Hooke, R. L., Gould, J. E., and Brzozowski, J.: Near-surface tem-peratures near and below the equilibrium line on polar and subpo-lar glaciers, Zeitschrift für Gletscherkunde und Glazialgeologie, 19, 1–25, 1983.

Hou, S. and Qin, D.: The effect of postdepositional process on the chemical profiles of snow pits in the percolation zone, Cold Regions Science and Technology, 34, 111–116, https://doi.org/10.1016/S0165-232X(01)00065-9, 2002.

Huss, M.: Density assumptions for converting geodetic glacier volume change to mass change, The Cryosphere, 7, 877–887, https://doi.org/10.5194/tc-7-877-2013, 2013.

Huss, M., Zemp, M., Joerg, P. C., and Salzmann, N.: High uncertainty in 21st century runoff projections from glacierized basins, Journal of Hydrology, 510, 35–48, https://doi.org/10.1016/j.jhydrol.2013.12.017, 2014.

Jordan, R., Albert, M., and Brun, E.: Snow and climate: physical processes, surface energy exchange and modeling, chapter Physical processes within the snow cover and their parameteriza tion, https://assets.cambridge.org/97805218/54542/frontmatter/9780521854542_frontmatter.pdf, 2008.

Kaser, G., Cogley, J. G., Dyurgerov, M. B., Meier, M. F., and Ohmura, A.: Mass balance of glaciers and ice caps: Consensus estimates for 1961–2004, Geophysical Research Letters, 33, 2006GL027 511, https://doi.org/10.1029/2006GL027511, 2006.

Kawashima, K. and Yamada, T.: Experimental studies on the transformation from firn to ice in the wet-snow zone of temperate glaciers, Annals of Glaciology, 24, 181–185, https://doi.org/https://doi.org/10.3189/S0260305500012143, 1997.

Knight, R., Tercier, P., and Irving, J.: The effect of vertical measurement resolution on the correlation structure of a ground penetrating radar reflection image, Geophysical Research Letters, 31, 2004GL021 112, https://doi.org/10.1029/2004GL021112, 2004.

Kohler, J., Moore, J., Kennett, M., Engeset, R., and Elvehøy, H.: Using ground-penetrating radar to image previous years' summer surfaces for mass-balance measurements, Annals of Glaciology, 24, 355–360, https://doi.org/10.3189/S0260305500012441, 1997.

Kronenberg, M., Barandun, M., Hoelzle, M., Huss, M., Farinotti, D., Azisov, E., Usubaliev, R., Gafurov, A., Petrakov, D., and Kääb, A.: Mass-balance reconstruction for Glacier No. 354, Tien Shan, from 2003 to 2014, Annals of Glaciology, 57, 92–102, https://doi.org/10.3189/2016AoG71A032, 2016.

Kruetzmann, N. C., Rack, W., McDonald, A. J., and George, S. E.: Snow accumulation and compaction derived from GPR data near Ross Island, Antarctica, The Cryosphere, 5, 391–404, https://doi.org/10.5194/tc-5-391-2011, 2011.

Kääb, A., Berthier, E., Nuth, C., Gardelle, J., and Arnaud, Y.: Contrasting patterns of early twenty-first-century glacier mass change in the Himalayas, Nature, 488, 495–498, https://doi.org/10.1038/nature11324, 2012.

Lambrecht, A., Mayer, C., Bohleber, P., and Aizen, V.: High altitude accumulation and preserved climate information in the western Pamir, observations from the Fedchenko Glacier accumulation basin, Journal of Glaciology, 66, 219–230, https://doi.org/10.1017/jog.2019.97, 2020.

https://doi.org/10.5194/egusphere-2025-615
Preprint. Discussion started: 28 March 2025

Li, J. and Zwally, H. J.: Modeling the density variation in the shallow firn layer, Annals of Glaciology, 38, 309–313, https://doi.org/10.3189/172756404781814988, 2004.

Ligtenberg, S. R. M., Helsen, M. M., and Van Den Broeke, M. R.: An improved semi-empirical model for the densification of Antarctic firn, The Cryosphere, 5, 809–819, https://doi.org/10.5194/tc-5-809-2011, 2011.

Ligtenberg, S. R. M., Kuipers Munneke, P., and Van Den Broeke, M. R.: Present and future variations in Antarctic firn air content, The Cryosphere, 8, 1711–1723, https://doi.org/10.5194/tc-8-1711-2014, 2014.

Looyenga, H.: Dielectric constants of heterogeneous mixtures, Physica, 31, 401–406, https://doi.org/10.1016/0031-8914(65)90045-5, 1965.

Lüthi, M. and Funk, M.: Dating ice cores from a high Alpine glacier with a flow model for cold firn, Annals of Glaciology, 31, 69–79, https://doi.org/10.3189/172756400781820381, 2000.

Machguth, H., Eisen, O., Paul, F., and Hoelzle, M.: Strong spatial variability of snow accumulation observed with helicopter-borne GPR on two adjacent Alpine glaciers, Geophysical Research Letters, 33, 2006GL026 576, https://doi.org/10.1029/2006GL026576, 2006.

Machguth, H., MacFerrin, M., Van As, D., Box, J. E., Charalampidis, C., Colgan, W., Fausto, R. S., Meijer, H. A. J., Mosley-Thompson, E., and Van De Wal, R. S. W.: Greenland meltwater storage in firn limited by near-surface ice formation, Nature Climate Change, 6, 390–393, https://doi.org/10.1038/nclimate2899, 2016.

Marchenko, S., Pohjola, V. A., Pettersson, R., Van Pelt, W. J. J., Vega, C. P., Machguth, H., Bøggild, C. E., and Isaksson, E.: A plot-scale study of firn stratigraphy at Lomonosovfonna, Svalbard, using ice cores, borehole video and GPR surveys in 2012–14, Journal of Glaciology, 63, 67–78, https://doi.org/10.1017/jog.2016.118, 2017.

Mayer, C., Lambrecht, A., Oerter, H., Schwikowski, M., Vuillermoz, E., Frank, N., and Diolaiuti, G.: Accumulation Studies at a High Elevation Glacier Site in Central Karakoram, Advances in Meteorology, 2014, 1–12, https://doi.org/10.1155/2014/215162, 2014.

MeteoSchweiz: Jahresverlauf an Stationen. Jungfraujoch, https://www.meteoswiss.admin.ch/services-and-publications/applications/measurement-values-and-measuring-networks.html#param=messnetz-automatisch&lang=en&station=JUN&chart=day&table=false&compare=n, accessed: 2024-04-06, 2024.

Moholdt, G., Nuth, C., Hagen, J. O., and Kohler, J.: Recent elevation changes of Svalbard glaciers derived from ICESat laser altimetry, Remote Sensing of Environment, 114, 2756–2767, https://doi.org/10.1016/j.rse.2010.06.008, 2010.

Murray, T., Booth, A., and Rippin, D. M.: Water-Content of Glacier-Ice: Limitations on Estimates from Velocity Analysis of Surface Ground-Penetrating Radar Surveys, Journal of Environmental and Engineering Geophysics, 12, 87–99, https://doi.org/10.2113/JEEG12.1.87, 2007.

Ohmura, A., Bauder, A., Müller, H., and Kappenberger, G.: Long-term change of mass balance and the role of radiation, Annals of Glaciology, 46, 367–374, https://doi.org/10.3189/172756407782871297, 2007.

Østrem, G. and Brugman, M.: Glacier mass-balance measurements: a manual for field and office work, Tech. Rep. 4, National Hydrology Research Institute, NHRI Science Report No. 4., 1991.

Parry, V., Nienow, P., Mair, D., Scott, J., Hubbard, B., Steffen, K., and Wingham, D.: Investigations of meltwater refreezing and density variations in the snowpack and firn within the percolation zone of the Greenland ice sheet, Annals of Glaciology, 46, 61–68, https://doi.org/10.3189/172756407782871332, 2007.

Pipes, A. and Quick, M. C.: UBC Watershed Model Users Guide, Department of Civil Engineering, University of British Columbia, Vancouver, British Columbia, Canada, 1977.

Porsani, J. L. and Sauck, W. A.: Ground-penetrating radar profiles over multiple steel tanks: Artifact removal through effective data processing, GEOPHYSICS, 72, J77–J83, https://doi.org/10.1190/1.2783412, 2007.

https://doi.org/10.5194/egusphere-2025-615
Preprint. Discussion started: 28 March 2025

Pälli, A., Moore, J. C., and Rolstad, C.: Firn–ice transition-zone features of four polythermal glaciers in Svalbard seen by ground-penetrating radar, Annals of Glaciology, 37, 298–304, https://doi.org/10.3189/172756403781816059, 2003.

Reeh, N.: A nonsteady-state firn-densification model for the percolation zone of a glacier, Journal of Geophysical Research: Earth Surface, 113, 2007JF000 746, https://doi.org/10.1029/2007JF000746, 2008.

Rennermalm, K., Hock, R., Covi, F., Xiao, J., Corti, G., Kingslake, J., Leidman, S. Z., Miège, C., Macferrin, M., Machguth, H., Osterberg, E., Kameda, T., and McConnell, J. R.: Shallow firn cores 1989–2019 in southwest Greenland's percolation zone reveal decreasing density and ice layer thickness after 2012, Journal of Glaciology, 68, 431–442, https://doi.org/10.1017/jog.2021.102, 2022.

Sapiano, J. J., Harrison, W. D., and Echelmeyer, K. A.: Elevation, volume and terminus changes of nine glaciers in North America, Journal of Glaciology, 44, 119–135, https://doi.org/10.3189/S0022143000002410, 1998.

Schiefer, E., Menounos, B., and Wheate, R.: Recent volume loss of British Columbian glaciers, Canada, Geophysical Research Letters, 34, 2007GL030 780, https://doi.org/10.1029/2007GL030780, 2007.

Schmelzbach, C., Tronicke, J., and Dietrich, P.: High-resolution water content estimation from surface-based ground-penetrating radar reflection data by impedance inversion, Water Resources Research, 48, 2012WR011 955, https://doi.org/10.1029/2012WR011955, 2012.

Schneider, T. and Jansson, P.: Internal accumulation in firn and its significance for the mass balance of Storglaciären, Sweden, Journal of Glaciology, 50, 25–34, https://doi.org/10.3189/172756504781830277, 2004.

Seligman, G.: The Structure of a Temperate Glacier, The Geographical Journal, 97, 295, https://doi.org/10.2307/1787399, 1941.

Shepherd, A., Ivins, E. R., A, G., Barletta, V. R., Bentley, M. J., Bettadpur, S., Briggs, K. H., Bromwich, D. H., Forsberg, R., Galin, N., Horwath, M., Jacobs, S., Joughin, I., King, M. A., Lenaerts, J. T. M., Li, J., Ligtenberg, S. R. M., Luckman, A., Luthcke, S. B., McMillan, M., Meister, R., Milne, G., Mouginot, J., Muir, A., Nicolas, J. P., Paden, J., Payne, A. J., Pritchard, H., Rignot, E., Rott, H., Sørensen, L. S., Scambos, T. A., Scheuchl, B., Schrama, E. J. O., Smith, B., Sundal, A. V., Van Angelen, J. H., Van De Berg, W. J., Van Den Broeke, M. R., Vaughan, D. G., Velicogna, I., Wahr, J., Whitehouse, P. L., Wingham, D. J., Yi, D., Young, D., and Zwally, H. J.: A Reconciled Estimate of Ice-Sheet Mass Balance, Science, 338, 1183–1189, https://doi.org/10.1126/science.1228102, 2012.

Sheriff, R. E. and Geldart, L. P.: Exploration Seismology, Cambridge University Press, 2nd edn., 1999.

Simonsen, S. B., Stenseng, L., Adalgeirsdottir, G., Fausto, R. S., Hvidberg, C. S., and Lucas-Picher, P.: Assessing a multilayered dynamic firn-compaction model for Greenland with ASIRAS radar measurements, Journal of Glaciology, 59, 545–558, https://doi.org/10.3189/2013JoG12J158, 2013.

Sinisalo, A., Grinsted, A., Moore, J. C., Kärkäs, E., and Pettersson, R.: Snow-accumulation studies in Antarctica with ground-penetrating radar using 50, 100 and 800 MHz antenna frequencies, Annals of Glaciology, 37, 194–198, https://doi.org/10.3189/172756403781815825, 2003.

Sold, L., Huss, M., Eichler, A., Schwikowski, M., and Hoelzle, M.: Unlocking annual firn layer water equivalents from ground-penetrating radar data on an Alpine glacier, The Cryosphere, 9, 1075–1087, https://doi.org/10.5194/tc-9-1075-2015, 2015.

Stevens, C. M., Verjans, V., Lundin, J. M. D., Kahle, E. C., Horlings, A. N., Horlings, B. I., and Waddington, E. D.: The Community Firn Model (CFM) v1.0, Geoscientific Model Development, 13, 4355–4377, https://doi.org/10.5194/gmd-13-4355-2020, 2020.

Stevens, C. M., Sass, L., Florentine, C., McNeil, C., Baker, E., and Bollen, K.: Direct measurements of firn-density evolution from 2016 to 2022 at Wolverine Glacier, Alaska, Journal of Glaciology, pp. 1–11, https://doi.org/10.1017/jog.2024.24, 2024.

Stocker, T. F., Qin, D., Plattner, G.-K., Tignor, M., Allen, S. K., Boschung, J., Naules, A., Xia, Y., Bex, V., and Midgley, P. M.: IPCC: Climate Change 2013: The Physical Science Basis, Con tribution of Working Group I to the Fifth Assessment Report of the Intergovernmental Panel on Climate Change, Tech. rep., Cambridge University Press, Cambridge, UK and New York, NY, USA, 2013.

https://doi.org/10.5194/egusphere-2025-615
Preprint. Discussion started: 28 March 2025

Topp, G. C., Davis, J. L., and Annan, A. P.: Electromagnetic determination of soil water content: Measurements in coaxial transmission lines, Water Resources Research, 16, 574–582, https://doi.org/10.1029/WR016i003p00574, 1980.

Ulriksen, C. P.: Application of Impulse Radar to Civil Engineering, Ph.D. thesis, Lund University of Technology, Lund, 1982.

van Pelt, W. J. J., Pettersson, R., Pohjola, V. A., Marchenko, S., Claremar, B., and Oerlemans, J.: Inverse estimation of snow accumulation along a radar transect on Nordenskiöldbreen, Svalbard, Journal of Geophysical Research: Earth Surface, 119, 816–835, https://doi.org/10.1002/2013JF003040, 2014.

Vaughan, D. G., Corr, H. F. J., Doake, C. S. M., and Waddington, E. D.: Distortion of isochronous layers in ice revealed by ground-penetrating radar, Nature, 398, 323–326, https://doi.org/10.1038/18653, 1999.

Waddington, E. D., Neumann, T. A., Koutnik, M. R., Marshall, H.-P., and Morse, D. L.: Inference of accumulation-rate patterns from deep layers in glaciers and ice sheets, Journal of Glaciology, 53, 694–712, https://doi.org/10.3189/002214307784409351, 2007.

Wake, L. M. and Marshall, S. J.: Assessment of current methods of positive degree-day calculation using in situ observations from glaciated regions, Journal of Glaciology, 61, 329–344, https://doi.org/10.3189/2015JoG14J116, 2015.

Wharton, R. P., Hazen, G. A., Rau, R. N., and Best, D. L.: Electromagnetic Propagation Logging: Advances in Technique and Interpretation, in: All Days, pp. SPE–9267–MS, SPE, Dallas, Texas, https://doi.org/10.2118/9267-MS, 1980.

Wingham, D. J., Ridout, A. J., Scharroo, R., Arthern, R. J., and Shum, C. K.: Antarctic Elevation Change from 1992 to 1996, Science, 282, 456–458, https://doi.org/10.1126/science.282.5388.456, 1998.

Winkler, M., Schellander, H., and Gruber, S.: Snow water equivalents exclusively from snow depths and their temporal changes: the Δsnow model, Hydrology and Earth System Sciences, 25, 1165–1187, https://doi.org/10.5194/hess-25-1165-2021, 2021.

Wouters, B., Martin-Español, A., Helm, V., Flament, T., Van Wessem, J. M., Ligtenberg, S. R. M., Van Den Broeke, M. R., and Bamber, J. L.: Dynamic thinning of glaciers on the Southern Antarctic Peninsula, Science, 348, 899–903, https://doi.org/10.1126/science.aaa5727, 2015.

Yilmaz, : Seismic Data Analysis: Processing, Inversion, and Interpretation of Seismic Data, Society of Exploration Geophysicists, ISBN 978-1-56080-094-1 978-1-56080-158-0, https://doi.org/10.1190/1.9781560801580, 2001.

Zelt, C. A. and Smith, R. B.: Seismic travel-time inversion for 2-D crustal velocity structure, Geophysical Journal International, 108, 16–34, 1992.

Zemp, M., Hoelzle, M., and Haeberli, W.: Six decades of glacier mass-balance observations: a review of the worldwide monitoring network, Annals of Glaciology, 50, 101–111, https://doi.org/10.3189/172756409787769591, 2009.

Zhao, W., Forte, E., Colucci, R. R., and Pipan, M.: High-resolution glacier imaging and characterization by means of GPR attribute analysis, Geophysical Journal International, 206, 1366–1374, https://doi.org/10.1093/gji/ggw208, 2016.

Zwally, H. J., Abdalati, W., Herring, T., Larson, K., Saba, J., and Steffen, K.: Surface Melt-Induced Acceleration of Greenland Ice-Sheet Flow, Science, 297, 218–222, https://doi.org/10.1126/science.1072708, 2002.

Zwally, H. J., Giovinetto, M. B., Li, J., Cornejo, H. G., Beckley, M. A., Brenner, A. C., Saba, J. L., and Yi, D.: Mass changes of the Greenland and Antarctic ice sheets and shelves and contributions to sea-level rise: 1992–2002, Journal of Glaciology, 51, 509–527, https://doi.org/10.3189/172756505781829007, 2005.